MOMENT MAGNITUDE ESTIMATION FOR LIQUEFACTION ASSESSMENT IN WESTERN TÜRKİYE

BATI TÜRKİYE'DE SIVILAŞMA DEĞERLENDİRMESİ İÇİN MOMENT BÜYÜKLÜK TAHMİNİ

GİZEM BOYRAZ

Prof. Dr. MUSTAFA ABDULLAH SANDIKKAYA

Supervisor

Submitted to

Graduate School of Science and Engineering of Hacettepe University

as a Partial Fulfillment to the Requirements

for the Award of the Degree of Master of Science

in Civil Engineering

2026

ABSTRACT

MOMENT MAGNITUDE ESTIMATION FOR LIQUEFACTION ASSESSMENT IN WESTERN TÜRKİYE

Gizem BOYRAZ

Master of Science, Civil Engineering

Supervisor: Prof. Dr. M. Abdullah Sandıkkaya

November 2026, 57 pages

Repeated static or dynamic loading causes an increase in pore water pressure within soils, leading to a significant reduction in strength and stiffness, which results in liquefaction. Therefore, accurate estimation of seismic demand is crucial in liquefaction potential assessments. Seismic demand is represented by the cyclic stress ratio (CSR), which depends on moment magnitude and ground motion parameters. In this study, different approaches to moment magnitude (M_w) were examined to determine the most suitable M_w for use in liquefaction assessments in Western Türkiye and a suitable approach was proposed based on the results obtained. Four methods are considered: characteristic magnitude (M_{char}), deaggregation-based magnitude (M_{deag}), fault contribution-based magnitude (M_{fault}) and liquefaction hazard-based magnitude (M_{liq}). Liquefaction triggering was assessed using a simplified procedure proposed by Youd et al. (2001). In addition to the classical liquefaction analysis proposed by Youd et al. (2001), an assessment was performed by normalizing the CSR values with the magnitude scaling factor (MSF) to better assess the effect of moment magnitude. The results show that the choice of moment magnitude significantly affects the seismic demand and thus the estimated liquefaction potential.

Keywords Liquefaction, magnitude scaling factor, seismic hazard analysis, cyclic stress ratio, peak ground acceleration.

ÖZET

BATI TÜRKİYE'DE SIVILAŞMA DEĞERLENDİRMESİ İÇİN MOMENT BÜYÜKLÜK TAHMİNİ

Gizem BOYRAZ

Yüksek Lisans, İnşaat Mühendisliği Bölümü

Tez Danışmanı: Prof. Dr. M. Abdullah Sandıkkaya

Kasım 2026, 57 sayfa

Tekrarlı statik veya dinamik yüklemeler, zeminlerde boşluk suyu basıncının artmasına ve buna bağlı olarak dayanım ve rijitliğin aşırı derecede azalmasına neden olarak sıvılaşmaya yol açar. Bu nedenle sıvılaşma potansiyeli değerlendirmelerinde sismik talebin doğru bir şekilde tahmin edilmesi önemlidir. Sismik talep momnent büyüklüğüne ve yer hareketi parametrelerine bağlı olan döngüsel gerilme oranı (CSR) ile temsil edilir. Bu çalışmada, Batı Türkiye'deki sıvılaşma değerlendirmelerinde kullanılacak en uygun moment büyüklüğünü (M_w) belirlemek amacıyla farklı moment büyüklüğü yaklaşımları incelenmiş ve elde edilen sonuçlara dayanarak uygun bir yaklaşım önerilmiştir. Dört yöntem ele alınmıştır: karakteristik büyüklük (M_{char}), ayrıştırmaya dayalı büyüklük (M_{deag}), fay katkısına dayalı büyüklük (M_{fault}) ve sıvılaşma tehlikesine dayalı büyüklük (M_{liq}). Sıvılaşma tetiklenmesi, Youd vd. (2001) tarafından önerilen basitleştirilmiş prosedür kullanılarak değerlendirilmiştir. Youd et al. (2001) tarafından önerilen klasik sıvılaşma analizine ek olarak, moment büyüklüğünün etkisini daha iyi değerlendirmek için CSR değerleri büyüklük ölçekleme faktörü (MSF) ile normalize edilerek bir değerlendirme yapılmıştır. Elde edilen sonuçlar, moment büyüklüğü seçiminin sismik talebi ve dolayısıyla tahmin edilen sıvılaşma potansiyelini önemli ölçüde etkilediğini göstermektedir.

Anahtar Kelimeler: Büyüklük ölçekleme faktörü, sıvılaşma, sismik tehlike analizi, döngüsel gerilme oranı, en yüksek yer ivmesi.

ACKNOWLEDGEMENTS

I would like to express my sincere gratitude to my advisor M. Abdullah Sandıkkaya, for his invaluable guidance, support and encouragement throughout this thesis.

I would like to thank the members of my Examining Committee Members, Prof. Dr. Berna Unutmaz, Prof. Dr. Alper Aldemir, Assoc. Prof. Dr. Bekir Özer Ay and Assoc. Prof. Dr. Özkan Kale, for their valuable comments.

Finally, I am deeply grateful to my family and friends for their continuous support, patience and encouragement throughout my academic journey.

TABLE OF CONTENTS

ABSTRACT i

ÖZET iii

ACKNOWLEDGEMENTS v

TABLE OF CONTENTS vi

LIST OF FIGURES viii

LIST OF TABLES x

SYMBOLS AND ABBREVIATIONS xi

1. INTRODUCTION 1

1.1 Scope of the Thesis 2

1.2 Literature Review 2

1.2.1 Magnitude Scaling Factors 3

1.2.2 Cyclic Stress Ratio 10

1.2.3 Liquefaction Analysis, Youd et.al. 2001 10

1.2.4 Seismic Hazard Analysis 10

1.2.5 Deaggregation of Seismic Hazard 13

1.3 Organization 13

2. STUDY AREA AND DATA 15

2.1 Seismic Resources in Western Türkiye 15

2.2 Soil Profile and Parameters 16

2.3 Study Sites 17

3. METHODOLOGY 20

3.1 Determination of Representative Moment Magnitude 20

3.1.1 Characteristic Moment Magnitude 20

3.1.2 Deaggregation-Based Moment Magnitude 21

3.1.3 Fault Contribution-Based Moment Magnitude 24

3.1.4 Liquefaction Hazard-Based Moment Magnitude 26

3.2. Liquefaction Analysis Procedure 28

3.2.1 Calculation of Cyclic Stress Ratio ……..…… 28
3.2.2 Calculation of Cyclic Resistance Ratio ……..……. 28
3.2.3 Other Corrections ……..….. 30
3.2.4 MSF-Corrected CSR Evaluation (CSR× iMSF) ……..……..... 31
4. RESULTS ……..... 33
4.1 The Effect of Magnitude Selection Methods on CSR×iMSF Values 38
5. CONCLUSION ……..……..... 44
5.1 Discussions and Recommendations for Future Work ……..……..…..... 45
REFERENCE ...……..... 46
APPENDIX ……..... 49
APPENDIX A – Seismic Hazard Analysis Outputs ……..… 49
APPENDIX B – Deaggregation Analysis Outputs ……..……..... 50
APPENDIX C – Fault Contribution Analysis Outputs ...…….……..... 52
APPENDIX D – Liquefaction Hazard-Based and Charachteristic M_w Outputs ...…..... 54
APPENDIX E – Comparison of M_w Values……..…… 55
CURRICULUM VITAE 57

LIST OF FIGURES

Figure 1.1. MSF relationships suggested by several researchers and the recommended MSF range from the 1996 NCEER Workshop (Youd et al., 1997) ……..…….…….....…. 5

Figure 1.2. Figure 1.2. MSF relation suggested by Kishida and Tsai (2014), revised from Boulanger and Idriss (2014) ……..……..……..... 8

Figure 1.3. Steps of PSHA (Adapted from Kramer, 1996) ……...……..... 12

Figure 2.1. Active tectonic plate boundaries and major fault lines in Türkiye (Rockwell et al. 2001) …….…..…..... 15

Figure 2.3. Geographical distribution of the selected study points across Western Türkiye ..…….…….…….…..... 18

Figure 3.1. Distribution of magnitude values obtained for the DD-1 level in the study field …….…….... 21

Figure 3.2. Distribution of magnitude values obtained for the DD-2 level in the study field …….……..... 21

Figure 3.3. Distribution of magnitude values obtained for the DD-1 level in the study field …….……..... 23

Figure 3.4. Distribution of magnitude values obtained for the DD-2 level in the study field …….……..... 23

Figure 3.5. Distribution of magnitude values obtained for the DD-1 level in the study field …….……..... 25

Figure 3.6. Distribution of magnitude values obtained for the DD-2 level in the study field …….……...… 25

Figure 3.7. Distribution of magnitude values obtained for the DD-1 level in the study field …….…….. .. 27

Figure 3.8. Distribution of magnitude values obtained for the DD-2 level in the study field …….……..... 27

Figure 3.9. Akkar et al. (2014) ground motion prediction equation ……...….. 32

Figure 3.10. Basic relationships used in determining M_{liq} values ……..... 32

Figure 4.1. Comparison of Deaggregation-Based and Liquefaction Hazard-Based Magnitudes for (a) DD-1 and (b) DD-2 hazard levels …….…….……..... 33

Figure 4.2. Comparison of Deaggregation-Based and Characteristic Magnitudes for (a) DD-1 and (b) DD-2 hazard levels ……..... 34
Figure 4.3. Comparison of Fault Contribution-Based and Characteristic Magnitudes for (a) DD-1 and (b) DD-2 hazard levels …….……..... 35
Figure 4.4. Comparison of Fault Contribution-Based and Deaggregation-Based Magnitudes for (a) DD-1 and (b) DD-2 hazard levels ……..…..... 36
Figure 4.5. Comparison of Fault Contribution-Based and Liquefaction Hazard-Based Magnitudes for (a) DD-1 and (b) DD-2 hazard levels ……..…..... 37
Figure 4.6. Variation of CSR×iMSF values with depth for M_{char} and M_{deag} methods at (a) DD-2 and (b) DD-1 hazard levels ……..……..... 39
Figure 4.7. Variation of CSR×iMSF values with depth for M_{fault} and M_{deag} methods at (a) DD-2 and (b) DD-1 hazard levels ……..…….....…… 40
Figure 4.8. Variation of CSR×iMSF values with depth for M_{char} and M_{fault} methods at (a) DD-2 and (b) DD-1 hazard levels …….…… 41
Figure 4.9. Variation of CSR×iMSF values with depth for M_{liq} and M_{deag} methods at (a) DD-2 and (b) DD-1 hazard levels ……..…….....… 42
Figure 4.10. Variation of CSR×iMSF values with depth for M_{fault} and M_{liq} methods at (a) DD-2 and (b) DD-1 hazard levels ……..…….…….... 43

LIST OF TABLES

Table 1.1. MSFs obtained by Arango (1996) considering distant liquefaction areas ……..…….....…… 4
Table 1.2. MSFs obtained by Arango (1996) based on the recommendations of Seed et al. (1975) ……..…….....…... 5
Table 1.3. Youd and Noble (1997a) suggestions for MSF ..……..…….....… 6
Table 1.4. MSF Relationships in the literature …….…..... 9
Table 2.1. A representative 20 m liquefiable soil profile used in the study ….……..…..... 17
Table 2.2. Locations and coordinates of the study sites in Western Türkiye ..……..... 19
Table 3.1. Corrections to SPT (after Skempton, 1986; as compiled by Robertson and Wride, 1998; adapted from Youd et al., 2001) ……..…….....… 30
Table 3.2. Uncertainty coefficients from Juang et al. (2008) and Akkar et.al. (2014) …..... 32

SYMBOLS AND ABBREVIATIONS

Symbols

a_{max}	Maximum acceleration in shearing direction
g	Gravitational acceleration
M_w	Moment magnitude
V_{s30}	Shear wave velocity at top 30 m
z	Depth
σ_v	Vertical total stress
σ_v	Vertical effective stress
r_d	Stress reduction factor
FS	Factor of safety
Pa	Atmospheric pressure
P_L	Probability of liquefaction
N_{eq}	Equivalent number of cycles
b	Slope parameter of the CRR–N relationship
S_a	Spectral acceleration
M_{char}	Characteristic moment magnitude
M_{deag}	Deaggregation-based moment magnitude
M_{fault}	Fault contribution-based moment magnitude
M_{liq}	Liquefaction hazard-based moment magnitude

Abbreviations

CSR	Cyclic Stress Ratio
CRR	Cylic Resistance Ratio
MSF	Magnitude Scaling Factor
DWF	Duration Weighting Factor
CSR×iMSF	Magnitude-Corrected Cyclic Stress Ratio
PGA	Peak (maximum) Horizontal Ground Acceleration
SPT	Standard Penetration Test
PSHA	Probabilistic Seismic Hazard Analysis
GMPE	Ground Motion Prediction Equation
DD-1	2% Probability of Exceedance in 50 Years
DD-2	10% Probability of Exceedance in 50 Years

1. INTRODUCTION

Earthquakes are one of the most destructive natural phenomenon affecting urban areas and people, especially in active tectonic regions. Besides severe ground shaking, earthquakes can lead to various hazards such as soil liquefaction and landslides. Among these, soil liquefaction is one of the most significant events during seismic events, particularly in saturated, loose-grained soils. Liquefaction is defined as the rapid increase in pore water pressures and the reduction of effective stresses to zero due to dynamic impact in water-saturated loose sandy soils (Kramer, 1996). When the rigidity and strength of the soil suddenly decrease, its bearing capacity drops and as a result, serious damage can occur to structures and infrastructure systems. Türkiye is located in a high seismic activity region containing numerous active fault lines and has been affected by many major earthquakes throughout its history. Examples of these earthquakes include those in Erzincan (1993), Gölcük and Düzce (1999), Van (2011) and Kahramanmaraş (2023). Analysis of the consequences of these earthquakes clearly reveals the severity of structural damage caused by liquefaction. Traditionally, liquefaction triggering has been assessed using deterministic procedures based on simplified relationships between cyclic stress ratio (CSR) and cyclic resistance ratio (CRR). One of the approaches commonly used in engineering practice is the "Simplified Method" developed by Seed and Idriss (1971). In this method, the cyclic resistance ratio (CRR) is referenced to a specific earthquake magnitude, and different earthquake magnitudes are accounted for using magnitude scaling factors (MSFs) (Seed & Idriss, 1971; Youd et. al., 2001). The use of such typical values may not fully reflect the variability of seismic sources and earthquake characteristics affecting a particular region and consequently does not adequately represent the liquefaction potential of the region. This situation has necessitated a re-examination of the methodological gap between seismic hazard analysis and geotechnical assessment in the literature.

In a tectonically complex country like Türkiye, with seismic sources having different characteristics in each region, choosing a deterministic (singular) magnitude can lead to misleading results by ignoring the uncertainty of seismic hazard. To overcome these limitations and obtain more realistic liquefaction analysis results, probabilistic approaches are increasingly being adopted. Therefore, in this study, moment magnitude (M_w) values estimated using various approaches for Western Türkiye were compared; and the differences

between the statistical results obtained from probabilistic seismic hazard analysis (PSHA) and the tectonic characteristics of the region were evaluated.

1.1 Scope of the Thesis

The core objective of this study is to estimate the moment magnitude to be utilized in liquefaction assessment for Western Türkiye using different approaches and to compare and evaluate the results obtained by using these values in liquefaction analyses. Four different magnitude selection approaches were adopted in this study: (i) characteristic magnitude (M_{char}), (ii) deaggregation-based magnitude (M_{deag}), (iii) fault contribution-based magnitude (M_{fault}) and (iv) liquefaction hazard-based magnitude (M_{liq}). The liquefaction method suggested by Youd et al. (2001) was performed using M_w values estimated with these four different approaches, and an evaluation was made by normalizing the CSR values with the magnitude scaling factor (MSF) to better assess the impact of moment magnitude.

The results were compared to examine the impact of moment magnitude selection on liquefaction. This study aims to ensure a more broad understanding of how moment magnitude estimation affects liquefaction potential assessments.

1.2 Literature Review

Especially in seismically hazardous regions, liquefaction is one of the most significant geotechnical events threatening structural safety. Standard methods used in liquefaction trigger analysis define seismic demand (CSR) through ground acceleration (PGA) and moment magnitude. However, while most studies in the literature focus on the acceleration parameter, the estimation of moment magnitude is often based on simplified assumptions. In regions with complex seismic sources, these simplified approaches can lead to erroneous calculations of liquefaction resistance, as earthquakes of varying magnitudes and different source-to-site distances influence the amplitude, duration, and number of cyclic loading cycles of ground motion. This situation has necessitated a re-examination of the methodological gap between seismic hazard analysis and geotechnical assessment in the literature. Aydoğan (2025) examines a probabilistic seismic hazard analysis based approach which was proposed to identify the moment magnitude to be utilized in liquefaction assessments. In the study, representative moment magnitudes corresponding to specific hazard levels were obtained using deaggregation analyses. Furthermore, it was emphasized

that the choice of moment magnitude can significantly affect the liquefaction analysis results through MSF. However, the comparative evaluation of different moment magnitude determination methods has remained limited.

1.2.1 Magnitude Scaling Factors

MSFs are important parameters used in determining liquefaction potential by including the cyclic loading effects of earthquakes in term of magnitude. MSFs reflect the features of applied seismic loadings and the soil's reaction and these factors have been developed based on fatigue behavior principles. Over time, based on field observations, laboratory experiments and probability analyses, different researchers have developed various MSF formulas constrained by soil type, experimental method and moment magnitude ranges. By applying MSF, engineers can more accurately predict the probability of liquefaction under earthquakes of different magnitudes, thus enabling safer design and risk assessment in high-risk earthquake zones. Seed and Idriss (1982) developed MSFs through laboratory tests on soils with different levels of constraint and they were used to scale the CRR baseline curves, generated for earthquakes of magnitude $M_w = 7.5$, to smaller or larger magnitudes. In safety factor calculations, MSF is expressed as follows through the relationship between CRR and CSR:

$$\mathrm{MSF} = \frac{\mathrm{CSR_M}}{\mathrm{CSR_{M7.5}}}$$

Idriss (1995) re-evaluated the data used in previous studies developed with Seed and found that an outlier data point used in the main analysis significantly affected the outcomes, which lead to lower than expected MSF values, particularly for earthquakes with magnitudes $M_w < 7.5$. As a conclusion of this evaluation, he suggested the following re-examined MSF relationships:

$$\mathrm{MSF} = \frac{10^{2.24}}{\mathrm{M_w}^{2.56}}$$

Idriss (1999) later introduced a set of Magnitude Scaling Factors.

$$MSF = 6.9 \times \exp\left(-\frac{M_w}{4}\right) - 0.058 \qquad MSF \leq 1.8$$

This proposed correlation was limited to an MSF value of at most 1.8 for small moment magnitudes and this upper limit corresponds approximately to earthquakes with a magnitude of $M_w \leq 5.2$.

Ambraseys (1988) improved empirical exponential equations determining CRR as a function of $(N_1)_{60}$ and M_w by analyzing field data. These factors are valid for estimating liquefaction hazard as they are based on field observations, but have not been widely used in engineering applications (Youd, 2001).

Arango (1996) formulated two sets of MSFs. The primary set depended on the furthest liquefaction impacts observed from the earthquake source and the average peak accelerations in those regions and this set is demonstrated in Table 1.1. The other set was created using energy concepts and Seed & Idriss (1982) relationships and is shown in Table 1.2.

Table 1.1. MSFs obtained by Arango (1996) considering distant liquefaction areas.

Earthquake magnitude	**Equivalent uniform number of cycles**	**Magnitude scaling factor**
8.25	38.4	0.63
8	26.7	0.75
7.5	15.0	1.00
7	9.6	1.25
6	3.8	2.00
5.5	1.7	3.00

Table 1.2. MSFs obtained by Arango (1996) based on the recommendations of Seed et al. (1975).

Earthquake magnitude	**Equivalent uniform number of cycles**	**Magnitude scaling factor**
8.5	26	0.76
7.5	15	1.0
6.75	10	1.22
6	5-6	1.65
5.25	2-3	2.45

Andrus and Stokoe (1997) plotted and improved limiting curves used in CRR calculations for M_w = 7.5 with studies of liquefaction resistance dependent on Vs and also determined limiting curves for areas where liquefaction was observed or not observed for earthquakes of magnitudes 6, 6.5 and 7. The curves are given in Figure 1.1. The MSFs are represented by the sequent equation:

$$\mathrm{MSF} = \left(\frac{\mathrm{M_w}}{7.5}\right)^{-2.56}$$

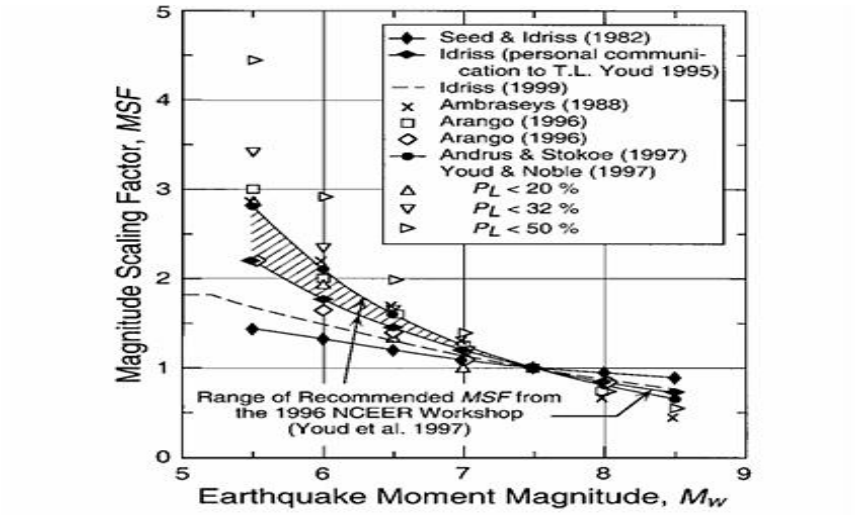


Figure 1.1 MSF relationships suggested by several researchers and the recommended MSF range from the 1996 NCEER Workshop (Youd et al., 1997).

Youd and Noble (1997a) analyzed field data using probabilistic (logistic) analysis and derived an equation from this analysis.

$$Q_L = \text{Logit}(P_L) = -7.0351 + 2.1738 \times M_w - 0.2678(N_1)_{60cs} + 3.0265 \times \ln \ln (CSR)$$

In this context $(N_1)_{60cs}$ is the blow count of corrected equivalent clean sand in an SPT test, PL is the probability of liquefaction. Youd and Noble (1997a) defined three sets of MSF sets for the probability of liquefaction. The sets improved for cases where the probability is less than 20%, 32% and 50% are shown in Table 1.3.

Table 1.3. Youd and Noble (1997a) suggestions for MSF.

M_w	**PL<20%**	**PL<32%**	**PL<50%**
5.5	2.86	3.45	4.44
6.0	1.93	2.35	2.92
6.5	1.34	1.65	1.99
7	0.96	1.19	1.39
7.5	-	-	1

The MSF values presented by Liu et al. (2001) were obtained not directly from a closed-form equation, but through an equivalent uniform cycle frame. Earthquake records were processed to determine the equivalent stress cycle number (N) and MSF values were calculated by normalizing these cycles to the reference magnitude ($M_w = 7.5$). In this context, empirical regression relationships incorporating the effects of magnitude (m), source distance (r), soil conditions and fracture orientation near the fault were proposed using earthquake records. In their study, Liu et al. presented the N-M_w relationship for three different "m" values (-0.37, -0.41 and -0.50) using a dataset of free-field records from 107 different earthquakes, considering components such as distance to fault rupture (R) and site type (S).

Kayen et al. (2013) developed an empirical correction factor (MSF) that describes the effect of different moment magnitudes on liquefaction potential using a probabilistic approach based on shear wave velocity data. The model is relevant for magnitudes $5.5 < M_w < 9.0$.

$$DWF = 15 \times M_w^{-1.342}$$

In the research conducted by Boulanger and Idriss (2008), the physical basis of magnitude scaling factors was re-examined. While most previous studies defined MSF solely through empirical relationships dependent on moment magnitude, this study emphasized that MSF essentially represents earthquake duration and cyclic loading effects. In this context, the approach of reducing irregular earthquake loadings to the equivalent number of cycles (N) was adopted and it was shown that MSF can be defined through the ratio of the number of cycles for a given magnitude to the number of cycles defined for the reference magnitude ($M_w = 7.5$). The study also revealed the determining effect of the parameter b, which defines the slope of the relationship between the cyclic resistance ratio and the number of cycles on MSF. A value of $b \approx 0.34$ was suggested for sandy soils and lower values were proposed for clay and plastic silts.

$$MSF = 1 + \left(0.65 \left(\frac{N_{M7.5}}{\left(\frac{3}{4}\right) \text{cycle}} \right)^{b} - 1 \right) \left(8.64 \exp \exp \left(-\frac{Mw}{4} \right) - 1.325 \right)$$

Here, 3/4 cycle represents the equivalent uniform loading at the maximum stress level for earthquakes characterized by a single strong cycle. Since the loading in such cases usually varies between 1/2 and 1 cycle, it is considered approximately 3/4 cycle.

Kishida and Tsai (2014) introduced an MSF relation involving the practical dependence of the soil parameter (b) defining the slope of the relation between CRR and the number of N to failure (Boulanger & Idriss, 2014, pp.114-115). The important impact of soil features on MSF relations is shown with Figure 1.2. based on MSF relations from Boulanger and Idriss (2014) and Kishida and Tsai (2014).

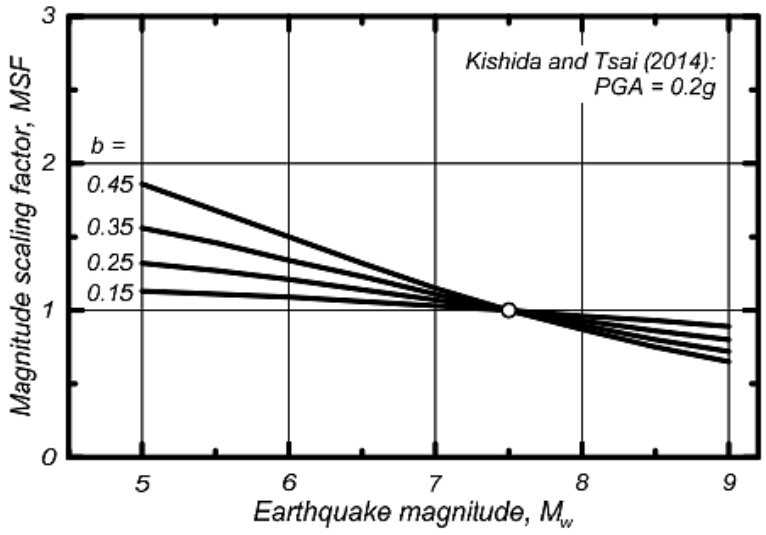


Figure 1.2. MSF relation suggested by Kishida and Tsai (2014), revised from Boulanger and Idriss (2014).

Unlike previous researchers, Çetin et al. (2018) developed an MSF relationship by utilizing probabilistic regression and maximum likelihood methods. Çetin et al. (2018) suggested the following equation of the moment magnitude correction factor to be applied to the repeated stress ratio.

$$\mathrm{MSF} = \left(\frac{\mathrm{M_w}}{7.5}\right)^{-2.324}$$

This relationship is valid for the range $5.5 \leq M_w \leq 8.4$ (Çetin & Bilge, 2012a). To conclude, the MSF values identified by several researchers in the literature are introduced in Table 1.4.

Table 1.4. MSF Relationships in the literature

Mw	Seed & Idriss 1982	Idriss 1995	Idriss 1999	Ambraseys 1988	Arango 1996		Andrus & Stokoe 1997	Youd & Noble 1997a			Liu et al. 2001			Cetin et al. 2004
					Distance	Energy		<20	<32	<50	Field	Lab.	Ave.	
5.5	1.43	2.20	1.69	2.86	3	2.20	2.78	2.86	3.45	4.44	1.84	1.72	1.77	1.99
6	1.32	1.76	1.48	2.20	2	1.65	2.09	1.93	2.35	2.92	1.60	1.52	1.57	1.64
6.5	1.19	1.44	1.30	1.69	1.60	1.40	1.60	1.34	1.65	1.99	1.38	1.36	1.37	1.37
7	1.08	1.19	1.14	1.30	1.25	1.10	1.26	0.94	1.19	1.39	1.18	1.18	1.18	1.17
7.5	1	1	1	1	1	1	1	0.70	0.88	1	1	1	1	1
8	0.94	0.84	0.88	0.67	0.75	0.85	0.81	—	—	0.73	0.83	0.83	0.83	0.87
8.5	0.89	0.72	0.77	0.44	—	—	0.66	—	—	0.56	0.76	0.76	0.76	0.76

1.2.2 Cyclic Stress Ratio

The seismic demand on soils is described by the seismic stress ratio, which is primarily characterized as cyclic stress ratio (Youd et. al., 2001). The CSR value, which is the seismic demand on a soil, appears as a fundamental parameter that expresses the ratio of the cyclic shear stress to the effective vertical stress in a soil layer under seismic influence. The equation introduced by Seed and Idriss (1997) is given below:

$$\mathrm{CSR} = 0.65 \times \frac{\mathrm{PGA}}{\mathrm{g}} \times \frac{\sigma_{\mathrm{v}}}{\sigma'_{\mathrm{v}}} \times \mathrm{r_d}$$

In this context, CSR refers to the cyclic stress ratio, in that, σ_{vo} and σ'_{vo} signify the total and effective vertical top load stresses under static conditions for the liquefiable layer, $\mathrm{a_{max}}$ presents the maximum ground acceleration (PGA) value [in g] and finally $\mathrm{r_d}$ represents the shear stress reduction factor.

1.2.3 Liquefaction Analysis, Youd et al. 2001

The liquefaction assessment method presented by Youd et al. (2001) is derived from the combined evaluation of field observations and laboratory data, building upon the results of the 1996 NCEER and 1998 NCEER/NSF workshops. In this method, liquefaction potential of soils is determined by comparing their liquefaction resistance (CRR) with the CSR generated during an earthquake. This method can be summarized as a modernized, data-driven and multi-domain test-supported improved version of the Simplified Method suggested by Seed and Idriss (1971) (Youd, 2001). In addition to the classical liquefaction analysis defined by Youd et al. (2001), an alternative assessment was performed by normalizing the CSR values with MSF to better assess the impact of moment magnitude.

1.2.4 Seismic Hazard Analysis

Analysis of seismic hazard is a critical process for evaluating future seismic potential in the design of engineering structures and regional risk management. In the literature, this process is addressed within two main methodological frameworks: deterministic (DSHA) and probabilistic (PSHA) (Kramer, 1996).

Kramer (1996), defining the place of these two approaches in engineering, states that the deterministic method focuses on the "worst-case scenario," while the probabilistic method presents probabilistic results by taking uncertainties into account. Cornell (1968) put forward PSHA methodology, which combines uncertainties in seismic sources and earthquake frequency within a mathematical framework. The PSHA process consists of identifying seismic sources, determining recurrence rates and calculating earthquake intensity through Earthquake Prediction Equations (GMPE) (Reiter, 1990). Today, data obtained from these analyses are used as a fundamental input not only in determining structural design accelerations but also in evaluating secondary effects such as soil liquefaction and seismically induced landslides (Youd et al., 2001). The development of probabilistic approaches in the last 20-30 years has allowed for the explicit consideration of uncertainties in moment magnitude, location and recurrence rate, as well as variations in ground motion parameters depending on moment magnitude and source-to-ground distance, in seismic hazard evaluations. PSHA method, developed in this context, offers a broad framework for identifying, quantitatively expressing and systematically combining these uncertainties. Thus, the seismic hazard in a given area can be assessed more logically and holistically (Kramer, 1996). The PSHA method is generally defined as a process consisting of four basic steps. This approach was systematically presented by Leon Reiter (1990).

The first step of PSHA involves identifying and characterizing earthquake sources that may affect the study area, as well as defining the probability distribution of possible rupture points that may occur within each source region.

It is generally assumed that earthquake occurrence has an equal probability at every point within the source region and the probability distribution of the source-site distance is determined using this assumption.

In the second step, the seismicity or temporal recurrence characteristics of earthquakes are determined for each earthquake source. For this purpose, earthquake recurrence relationships are used to determine the average exceedance rate of an earthquake of an accurate magnitude and are used to define the earthquake-generating potential of each source region.

In the third step, the ground motion parameters that earthquakes of several magnitudes and various source-site distances will create in the study area are determined using estimation relationships. The statistical uncertainties contained in these estimation relationships are also taken into account within the scope of PSHA.

In the final stage, the earthquake location, moment magnitude and uncertainties in the ground motion estimation are combined to evaluate the probability of the parameter of ground motion exceeding a certain value within a specific time interval.

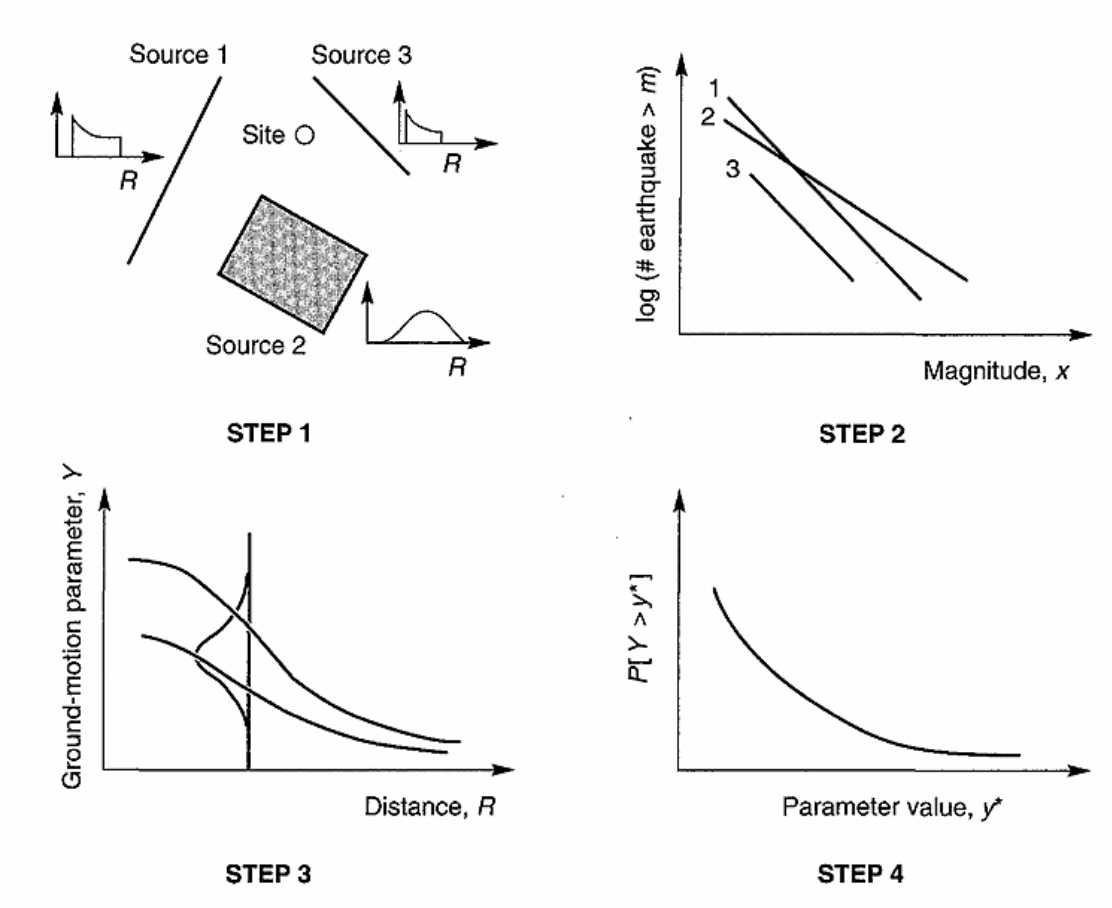


Figure 1.3. Steps of PSHA (Adapted from Kramer, 1996).

Seismic hazard analysis outputs provide PGA and SA values, in addition to exceedance probabilities at different periods for each study area. In this study, PGA values corresponding to a 50-year exceedance probability of 10% and 2% exceedance probabilities were used to represent DD-2 and DD-1 hazard levels, respectively. These parameters are attained from PSHA and are used as input in calculating CSR, which represents the seismic demand on the

ground. The resulting CSR values are adjusted using MSF to regard to the impact of moment magnitude in liquefaction assessments.

1.2.5 Deaggregation of Seismic Hazard

Deaggregation is a statistical deaggregation process used to show the relative contributions of magnitude, distance and ground motion variability to a hazard (McGuire, 2004). Seismic hazard deaggregation is an approach used in probabilistic seismic hazard analysis to determine which earthquake scenarios contribute to the total hazard. This approach examines the relative contributions of parameters including to moment magnitude (M), source-site distance (R) and epsilon (ε) that contribute to overlapping a certain ground motion level in a study area. This reveals the magnitude and distance combinations that most significantly affect the calculated total seismic hazard and allows for the identification of the controlling earthquake scenario that most affects ground motion in the study area. Seismic hazard deaggregation is a highly important in engineering applications, particularly in interpreting ground motion predictions and determining characteristic moment magnitudes used in liquefaction analyses (McGuire, 2004).

1.3 Organization

Chapter 1 presents the literature review and the scope of the thesis.

Chapter 2 defines the study field and presents geological, seismic and fault data, along with ground motion parameters and soil properties.

Chapter 3 estimates the earthquake moment magnitude using different approaches and analyzes the liquefaction potential for each M_w value by calculating the cyclic stress ratio. These approaches include liquefaction hazard-based M_w, deaggregation-based M_w, fault contribution-based M_w and the maximum magnitude of nearby faults. Liquefaction potentials were calculated using Youd et al. 2001.

Chapter 4 compares the values obtained from different M_w approaches through graphs and evaluates their effects on liquefaction demand.

Chapter 5 is the conclusion section of the thesis. The findings are interpreted, recommendations are made for the best M_w value that can be used in liquefaction analysis and suggestions are made for later studies.

2. STUDY AREA AND DATA

2.1 Seismic Resources in Western Türkiye

Influenced by the seismic dynamics regarding to the movements of the African continent and the Arabian Peninsula, as well as the movements of the European and Asian continents, Anatolia has faced major earthquakes. Although not part of the North Anatolian Fault System (NAF), the largest fault system, the Western Anatolian Region has widespread seismic activity and is one of the regions showing the greatest dynamism in the world (İnce ve Yılmazoğlu, 2021).

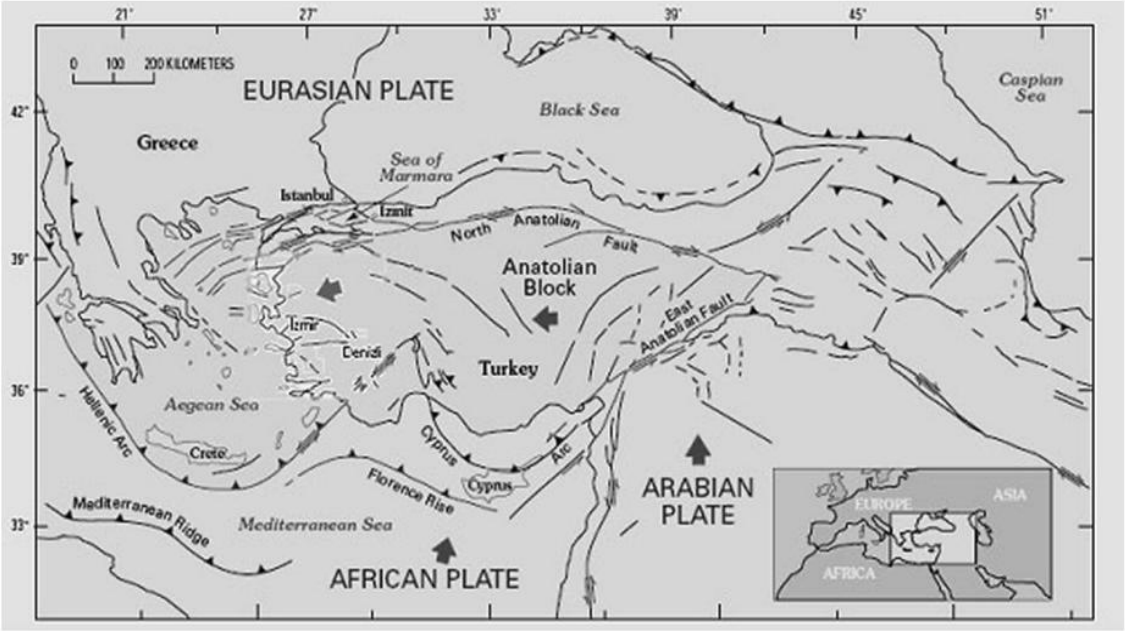


Figure 2.1. Active tectonic plate boundaries and major fault lines in Türkiye (Rockwell et al. 2001)

If the seismic sources in Western Anatolia are summarized under three groups that determine the tectonic structure of the region, the first and most dominant group consists of large east-west trending graben systems that are the product of north-south extension. These systems, such as the Gediz, Büyük Menderes and Küçük Menderes, consist of shallow-focus normal faults capable of producing high-magnitude earthquakes (Bozkurt, 2001). These faults form the main backbone of the topography and seismic motions in the field.

The second group consists of north-south trending strike-slip transfer faults that cut through or connect these graben systems. In particular, faults such as Tuzla and Seferihisar, located within the Izmir-Balıkesir Transfer Zone (IBTZ), are critical seismic sources that accommodate block rotations in the region (Sözbilir et al., 2016).

Finally, large-scale sources such as the southern branches of the North Anatolian Fault (NAF) are located on the northern boundary of the region, while the Hellenic Arc is situated on the southwestern coast. Faults such as Yenice-Gönen and Manyas carry the characteristic right lateral strike slip motion of the NAF to Western Anatolia (Emre et al., 2013), while subduction zones in the marine area are considered external seismic sources affecting the region in terms of both long-range earthquakes and tsunami risk.

In conclusion, seismic sources in Western Türkiye exhibit a complex structure consisting of highly active fault segments controlled by both normal faults associated with extensional tectonics and strike-slip fault systems. These characteristics constitute the main reason for the high seismic hazard potential of the region (Emre et al., 2018). Therefore, the representation of seismic sources is critical for hazard assessment and liquefaction analyses.

In this study, seismic source characterization is based on datasets obtained from the current fault database of MTA and AFAD. These resources provide information on fault geometry, segmentation and expected maximum magnitudes, which are necessary for probabilistic seismic hazard analysis.

2.2 Soil Profile and Parameters

The soil profile used in this study is derived from field investigation data and laboratory measurements. The profile consists of multiple soil layers extending to a depth of approximately 20 meters, with varying geotechnical properties. The groundwater table is assumed at the ground surface (GWT = 0 m), indicating fully saturated soil conditions throughout the profile.

The values of $(N_1)_{60}$ range approximately between 10 and 30, indicating predominantly loose to medium dense soil conditions, which are generally susceptible to liquefaction. Unit weights of soil vary between approximately 16–18 kN/m³ and fines content is considered

through correction factors applied in the analysis. These parameters are used as inputs for PSHA, deaggregation and subsequent liquefaction assessments. The soil profile used is demonstrated in Figure 2.1.

Table 2.1. A representative 20 m liquefiable soil profile used in the study.

γ_d : 18	γ_{sat} : 18	GWT: 0 m
Profile	**Depth**	**N**
1	1.5	14
1	3	10
1	4.5	20
1	6	11
1	7.5	12
1	9	11
1	10.5	12
1	12	11
1	13.5	10
1	15	12
1	16.5	11
1	18	12
1	19.5	13

2.3 Study Sites

The study area encompasses Western Türkiye, which has a highly active tectonic regime. 50 distinct analysis points have been selected to represent the variable seismic conditions in the region. These points were determined by taking into account their distance from fault sources, with each fault being represented by at least two points. This number was deemed sufficient to capture the diversity of faults present within the study area. The spatial distribution of the selected areas is shown in Figure 2.3. These locations are distributed along

major tectonic structures and surrounding fault zones. The selected points aim to capture the variability in seismic hazard and soil conditions across Western Türkiye.

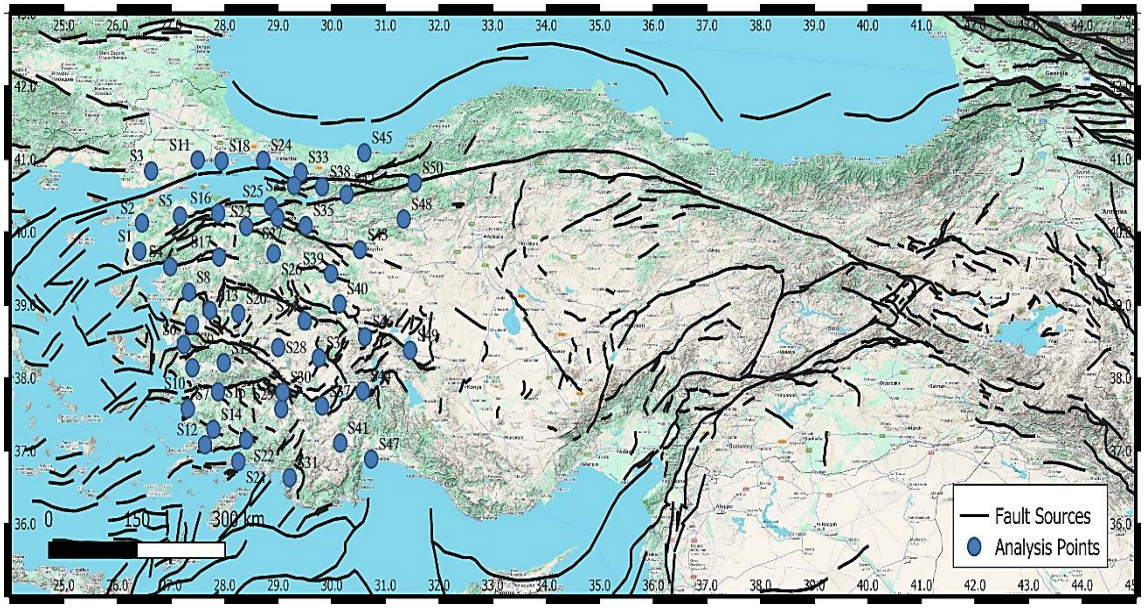


Figure 2.3. Geographical distribution of the selected study points across Western Türkiye.

The selection of these areas allows for a comprehensive evaluation of different moment magnitude estimation approaches under varying seismic and geological conditions. The coordinates and location information of the study areas researched in the analyses are given in Table 2.2.

Table 2.2. Locations and coordinates of the study sites in Western Türkiye.

Lon	Lat	siteID	Location
30.62	38.56	10301	Afyonkarahisar Şuhut
31.34	40.18	10601	Ankara Nallıhan
30.16	37.11	10701	Antalya Korkuteli
30.74	36.89	10702	Antalya Muratpaşa
27.88	37.81	10901	Aydın
27.32	37.58	10902	Aydın Söke
27.90	39.66	11001	Balıkesir
26.99	39.53	11002	Balıkesir Burhaniye
27.88	40.26	11003	Balıkesir Bandırma
31.55	40.68	11401	Bolu
29.82	37.61	11501	Burdur Orhanlı
28.40	40.08	11601	Bursa Mustafakemalpaşa
28.86	40.35	11602	Bursa Mudanya
28.92	39.70	11603	Bursa Büyükorhan
28.99	40.20	11604	Bursa Nilüfer
29.51	40.09	11605	Bursa İnegöl
26.46	40.12	11701	Çanakkale
26.41	39.74	11702	Çanakkale Ezine
27.17	40.22	11703	Çanakkale Biga
29.06	37.57	12001	Denizli Tavas
29.08	37.80	12002	Denizli Merkezefendi
29.76	38.28	12003	Denizli Çivril
26.63	40.84	12201	Edirne Keşan
30.52	39.76	12601	Eskişehir Odunpazarı
30.58	37.82	13201	Isparta
28.72	40.99	13401	İstanbul Avcılar
27.24	38.46	13501	İzmir Bornova
27.33	39.17	13502	İzmir Bergama
27.40	38.14	13503	İzmir Torbalı
27.99	38.21	13504	İzmir Ödemiş
29.42	40.82	14101	Kocaeli Gebze
29.82	40.62	14102	Kocaeli Gölcük
31.46	38.38	14201	Konya Akşehir
29.99	39.43	14301	Kütahya
30.14	39.02	14302	Kütahya Genişler
27.39	38.73	14501	Manisa
27.73	38.92	14502	Manisa Akhisar
28.26	38.88	14503	Manisa Gördes
27.63	37.08	14801	Muğla Bodrum
27.79	37.29	14802	Muğla Milas
28.26	36.85	14803	Muğla Marmaris
28.40	37.15	14804	Muğla Menteşe
29.21	36.63	14805	Muğla Fethiye
30.28	40.52	15401	Sakarya Geyve
30.61	41.09	15402	Sakarya Karasu
27.50	40.99	15901	Tekirdağ Süleymanpaşa
27.94	40.98	15902	Tekirdağ Marmara Ereğlisi
29.50	38.78	16401	Uşak
29.00	38.42	16402	Uşak Eşme
29.30	40.64	17701	Yalova

3. METHODOLOGY

3.1 Determination of Representative Moment Magnitude

3.1.1 Characteristic Moment Magnitude ($\mathbf{M_{char}}$)

In this study, all active faults within a 200 km radius of the study area were identified to determine the moment magnitude for liquefaction assessment and thus define the seismic demand. The maximum moment magnitude that each fault can generate was estimated based on its geological and geometric characteristics. Among these, the fault capable of generating the largest earthquake was selected as the controlling seismic source. This source was defined as a characteristic moment magnitude (M_{char}) to represent the maximum seismic potential of the faults surrounding each region.

$$M_{char} = (M_i)$$

where M_i represents the moment magnitude of each fault acting on the site under consideration.

This approach assumes that the largest possible earthquake governs the seismic demand and provides a conservative estimate for liquefaction triggering analysis. Therefore, M_{char} represents the worst-case scenario in terms of seismic loading. The distribution of the magnitude values obtained through this method for the DD-1 and DD-2 levels across the study area is presented in Figure 3.1 and Figure 3.2.

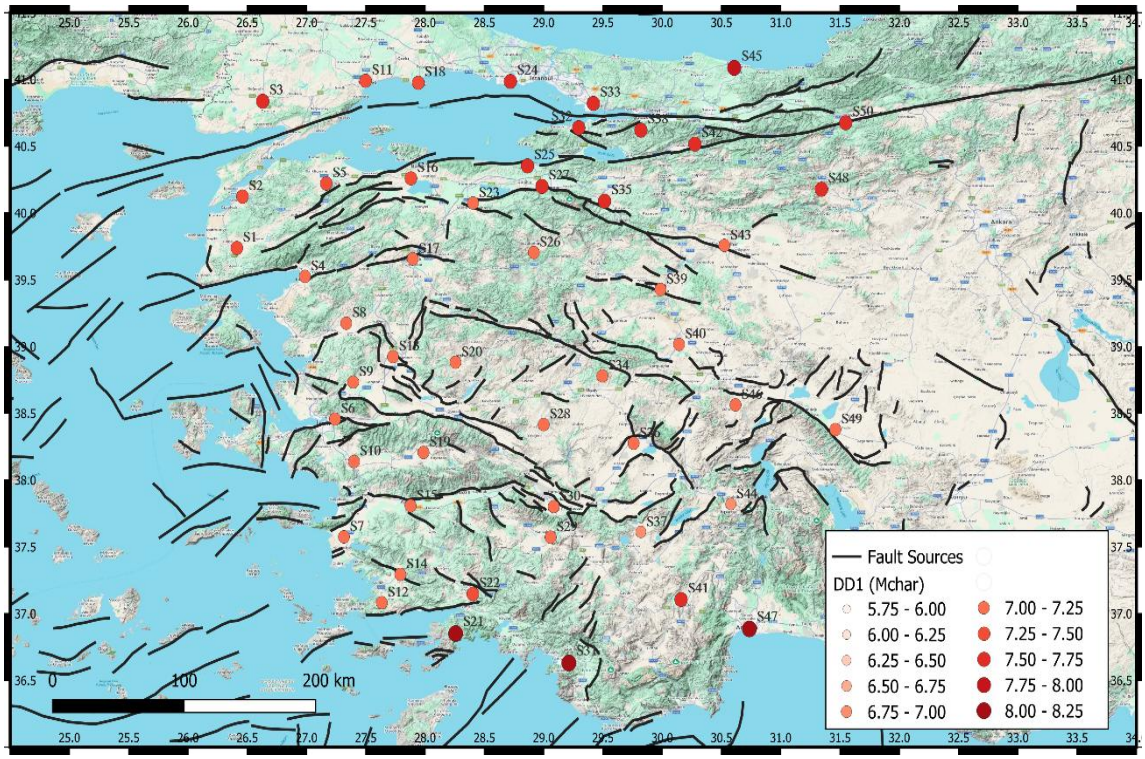


Figure 3.1. Distribution of magnitude values obtained for the DD-1 level in the study field.

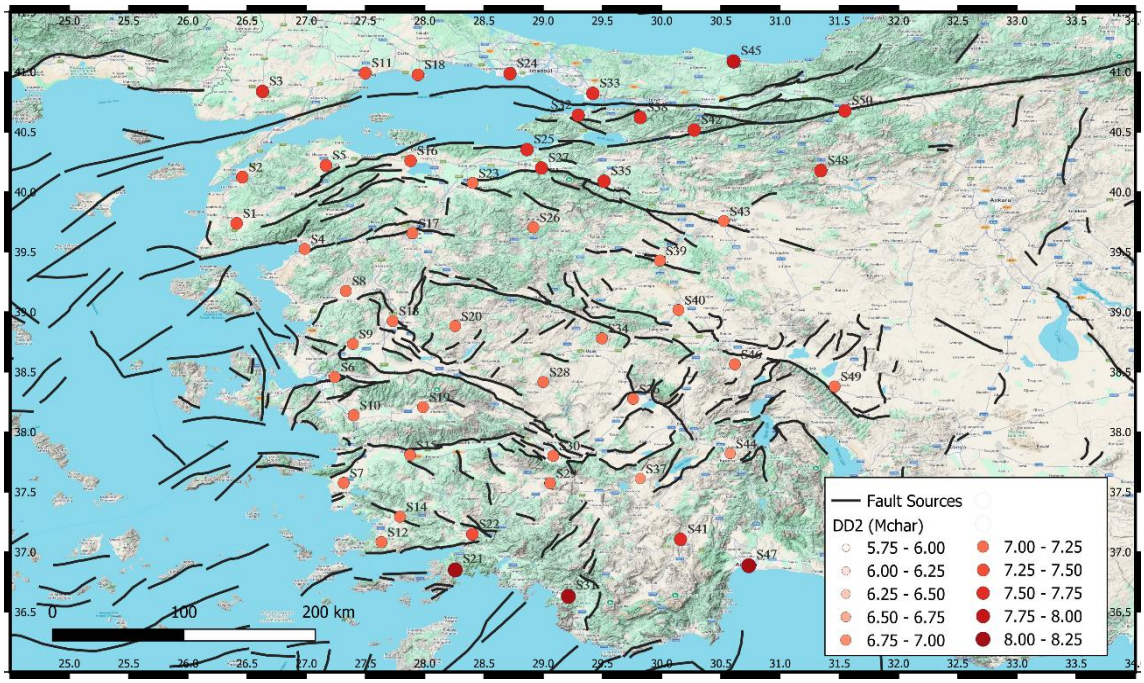


Figure 3.2. Distribution of magnitude values obtained for the DD-2 level in the study field.

3.1.2 Deaggregation-Based Moment Magnitude ($\mathbf{M_{deag}}$)

Deaggregation is the analysis of seismic hazard relating to a specific probability of exceedance based on combinations of moment magnitude and source-distance (Cornell, 1968). This provides information in terms of magnitude, distance and epsilon about the dominant earthquake scenarios contributing to seismic hazard in a given area. In this approach, after PSHA, hazard deaggregation is performed to identify the earthquake scenarios that make the most significant contribution to seismic hazard in the study field. From the outcomes of the deaggregation analysis, combinations of magnitude, distance and epsilon values that make the most significant contribution to seismic hazard were obtained and based on these results, a representative moment magnitude controlling the seismic hazard in the region was estimated. For each hazard level, the maximum value among the mean and modal magnitudes obtained from the deaggregation analyses based on PGA, SA(0.2) and SA(1.0) was used as the representative magnitude:

$$M_{max} = \max\left(M_{mean,PGA}, M_{mean,SA(0.2)}, M_{mean,SA(1.0)}, M_{mode,PGA}, M_{mode,SA(0.2)}, M_{mode,SA(1.0)}\right)$$

where M_{max} represents the maximum magnitude of the contributing earthquake scenarios derived from the hazard deaggregation. The distribution of the magnitude values obtained through this method for the DD-1 and DD-2 levels across the study area is presented in Figure 3.3 and Figure 3.4.

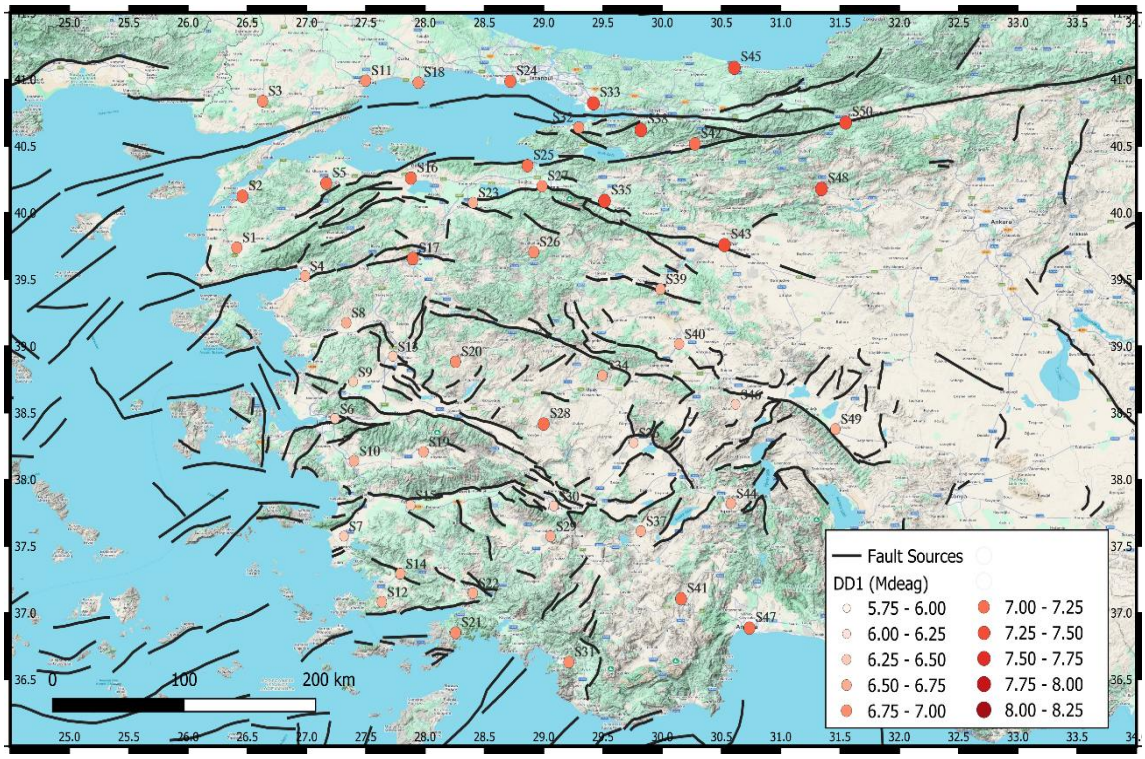


Figure 3.3. Distribution of magnitude values obtained for the DD-1 level in the study field.

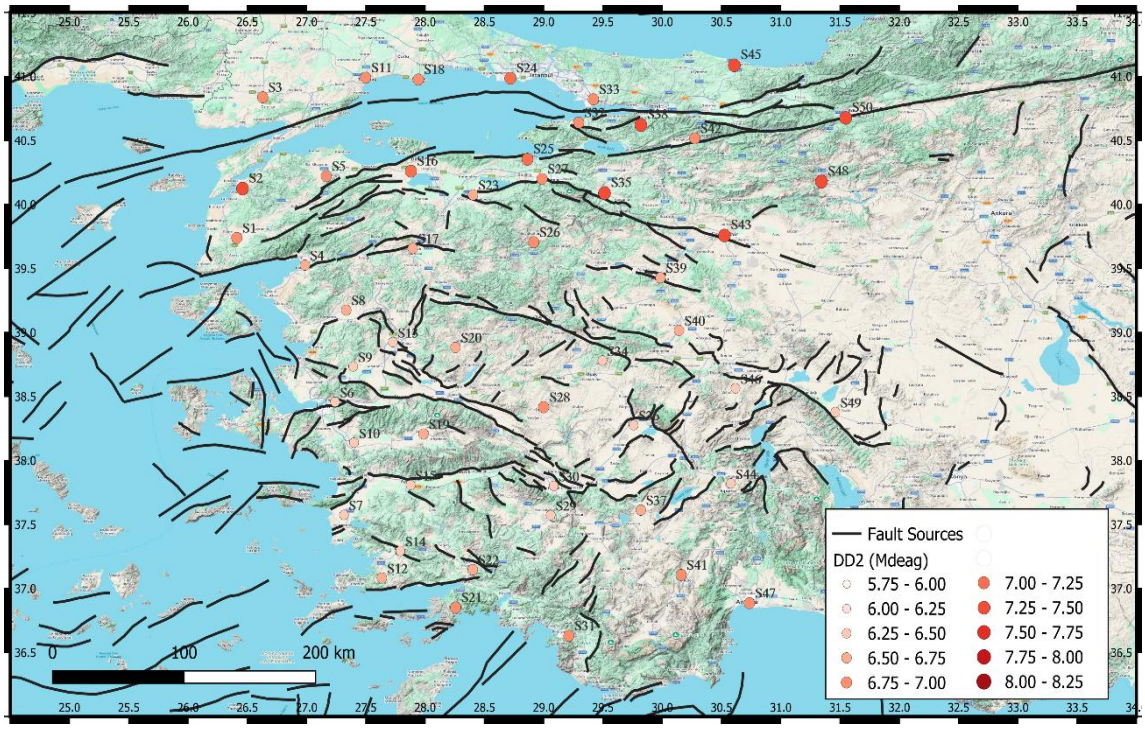


Figure 3.4. Distribution of magnitude values obtained for the DD-2 level in the study field.

3.1.3 Fault Contribution-Based Moment Magnitude (M_{fault})

As a third method, a fault contribution-based approach was used to determine a representative moment magnitude for liquefaction analysis. This approach takes into account the relevant contribution of each seismic source to the total hazard. In this approach, when determining the earthquake magnitude for a study area, the assessment is not based solely on the fault with the potential to generate the largest earthquake; rather, all active faults contributing to the seismic hazard in the region are evaluated collectively. The earthquake magnitude for each fault is weighted according to its contribution to the seismic hazard, resulting in a design magnitude specific to the study area. In this method, the weighted average moment magnitude, which will be used as the basic input in liquefaction analysis, is calculated using the proportional contributions of different seismic sources (faults) affecting the region to the total seismic hazard. For each site, the contributions of individual fault sources were obtained from the outcomes of PSHA. These contributions represent the relative impact of each fault on the seismic demand in the field.

The representative magnitude is denoted as M_{fault} and is calculated as a weighted average of the magnitudes of all contributing faults, where the weights correspond to their respective hazard contributions:

$$M_{fault} = \frac{\sum(M_i \cdot w_i)}{\sum w_i}$$

where M_i is the moment magnitude of the i-th fault and w_i is the contribution of that fault to the seismic hazard.

This approach ensures that faults contributing more to the hazard have a greater impact on the resulting representative magnitude. Therefore, it provides a more physically consistent estimate compared to choosing a single maximum or average magnitude and is considered a balanced representation between conservative and representative approaches. The distribution of the magnitude values obtained through this method for the DD-1 and DD-2 levels across the study area is presented in Figure 3.5 and Figure 3.6

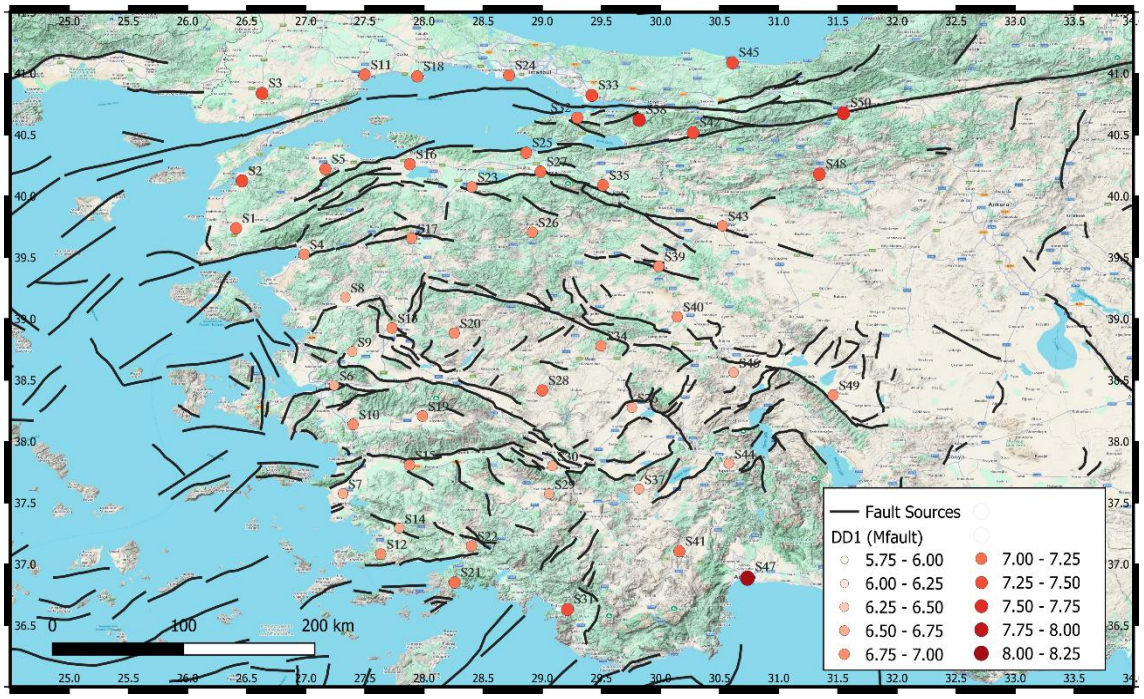


Figure 3.5. Distribution of magnitude values obtained for the DD-1 level in the study field.

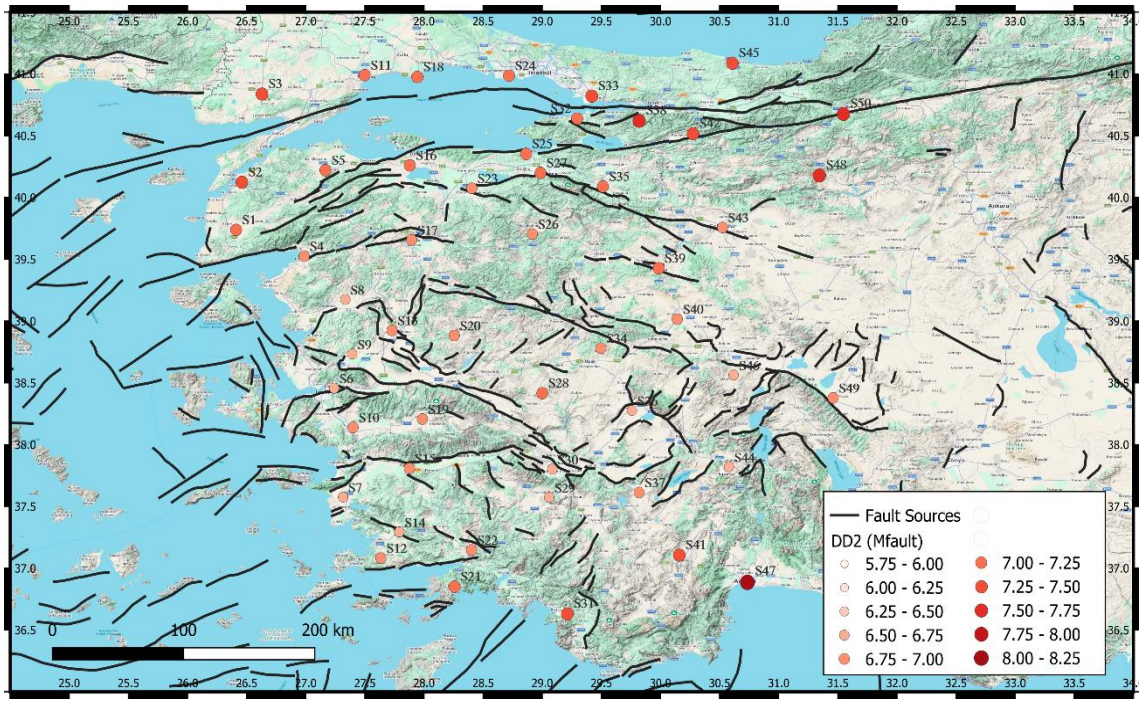


Figure 3.6. Distribution of magnitude values obtained for the DD-2 level in the study field.

3.1.4 Liquefaction Hazard–Based Moment Magnitude (M_{liq})

The uncertainties of the input parameters used in the CSR calculation were defined by coefficients of variation as suggested by Juang et al. (2008b) and converted to standard deviations. The uncertainty associated with PGA was obtained from the ground motion prediction model of Akkar et al. (2014) and combined with the uncertainties of the remaining CSR input parameters. The resulting CSR uncertainty was then included in the probabilistic liquefaction hazard analysis. Subsequently, three separate probabilistic hazard analyses were performed: First, a conventional PGA-based PSHA was conducted to quantify the ground motion hazard and its associated uncertainty. Second, a probabilistic liquefaction hazard analysis was performed using CSR as the hazard parameter, without considering the moment magnitude effect. Third, a probabilistic liquefaction hazard analysis was conducted using the magnitude-corrected cyclic stress ratio (CSR×iMSF), thereby incorporating the cyclic impacts of moment magnitude. The magnitude scaling factor was obtained from the ratio of CSR values corresponding to the same deviation probability in the two hazard curves. Finally, the moment magnitude was determined by applying the inverse solution of the MSF relationship.

Although M_{liq} is a consistent moment magnitude because it is theoretically derived directly from probabilistic liquefaction hazard analysis, its reliance on PGA-based hazard curves systematically leads to lower equivalent magnitudes. This reflects the limitations of PGA in representing earthquake duration and cyclic loading effects that trigger liquefaction. The distribution of the magnitude values obtained through this method for the DD-1 and DD-2 levels across the study area is presented in Figure 3.7 and Figure 3.8.

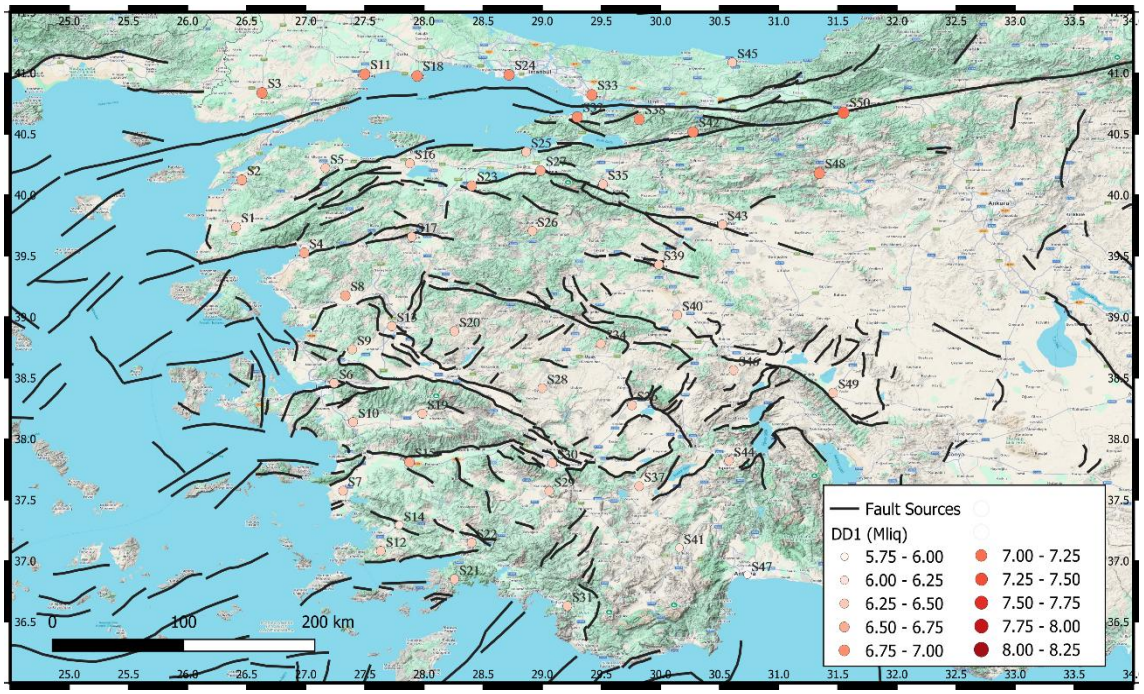


Figure 3.7. Distribution of magnitude values obtained from the DD-1 level in the study field.

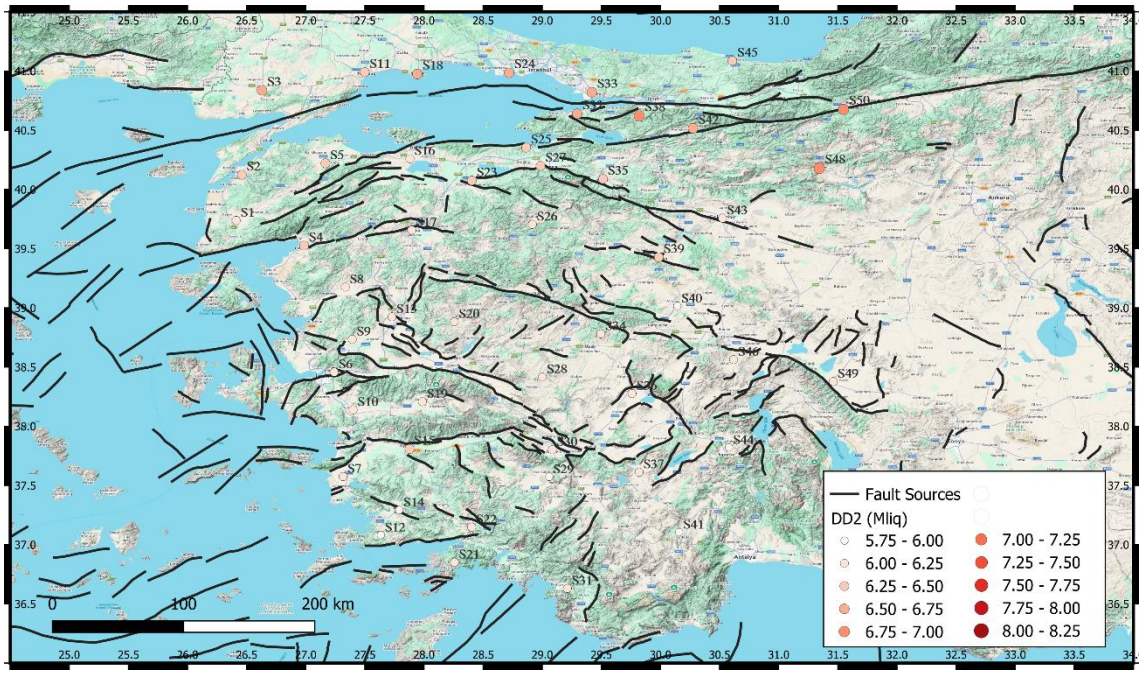


Figure 3.8. Distribution of magnitude values obtained from the DD-2 level in the study field.

In this study, four different magnitude selection approaches were adopted: (i) the characteristic magnitude representing the maximum seismic potential (M_{char}), (ii) the deaggregation-based representative magnitude reflecting the most probable earthquake scenario (M_{deag}), (iii) the fault contribution-based magnitude incorporating the relative influence of individual faults (M_{fault}) and (iv) the liquefaction hazard-based magnitude (M_{liq}). These approaches were compared to evaluate their impact on liquefaction triggering analysis. The magnitudes obtained from these methods were then used in magnitude scaling factor calculations to adjust the cyclic stress ratio for liquefaction analyses.

3.2. Liquefaction Analysis Procedure

3.2.1 Calculation of Cyclic Stress Ratio

The CSR value, the seismic demand on a soil layer, is one of the two main parameters that need to be calculated to evaluate the liquefaction resistance of soils. The equation developed by Seed and Idriss is used.

$$CSR = \left(\frac{\tau_{av}}{\sigma'_{vo}}\right) = 0.65 \times \left(\frac{a_{max}}{g}\right) \times \left(\frac{\sigma_{vo}}{\sigma'_{vo}}\right) \times r_d$$

The following equations can be used to predict average values of r_d (Liao and Whitman 1986b):

$$r_d = 1.0 - 0.00765z \quad \text{for} \leq 9.15\ \text{m}$$
$$r_d = 1.174 - 0.0267z \quad \text{for}\ 9.15\ \text{m} < z \leq 23\ \text{m}$$

where z is the depth below ground surface in meters.

3.2.2 Calculation of Cyclic Resistance Ratio

$$CRR_{7.5} = \frac{1}{34 - (N_1)_{60}} + \frac{(N_1)_{60}}{135} + \frac{50}{[10 \times (N_1)_{60} + 45]^2} - \frac{1}{200}$$

For this equation to be usable, the condition $(N_1)_{60} < 30$ must be met. For $(N_1)_{60} \geq 30$, clean-grained soils are categorized as non-liquefiable because they are too dense to liquefy.

The following equations were used to correct $(N_1)_{60}$ to the equivalent clean sand value $(N_1)_{60cs}$:

$$(N_1)_{60cs} = \alpha + \beta(N_1)_{60}$$

where α and β = coefficients identified from the following relationships:

$$\alpha = 0 \text{ for } FC \leq 5\ \%$$

$$\alpha = \exp\exp\left[1.76 - \left(\frac{190}{FC^2}\right)\right] \quad \text{for } 5\% < FC < 35\%$$

$$\alpha = 5.0 \quad \text{for } FC \geq 35\%$$

$$\beta = 1.0 \quad \text{for } FC \leq 5\%$$

$$\beta = \exp\exp\left[0.99 + \left(\frac{FC^{1.5}}{1{,}000}\right)\right] \quad \text{for } 5\% < FC < 35\%$$

$$\beta = 1.2 \quad \text{for } FC \geq 35\%$$

3.2.3 Other Corrections

Table 3.1. Corrections to SPT (after Skempton, 1986; as compiled by Robertson and Wride, 1998; adapted from Youd et al., 2001)

Factor (1)	Equipment variable (2)	Term (3)	Correction (4)
Overburden pressure	—	C_N	$\left(\frac{P_a}{\sigma'_{v0}}\right)^{0.5}$
Overburden pressure	—	C_N	$C_N \leq 1.7$
Energy ratio	Donut hammer	C_E	0.5–1.0
Energy ratio	Safety hammer	C_E	0.7–1.2
Energy ratio	Automatic-trip Donut-type hammer	C_E	0.8–1.3
Borehole diameter	65–115 mm	C_B	1.0
Borehole diameter	150 mm	C_B	1.05
Borehole diameter	200 mm	C_B	1.15
Rod length	<3 m	C_R	0.75
Rod length	3–4 m	C_R	0.8
Rod length	4–6 m	C_R	0.85
Rod length	6–10 m	C_R	0.95
Rod length	10–30 m	C_R	1.0
Sampling method	Standard sampler	C_S	1.0
Sampling method	Sampler without liners	C_S	1.1–1.3

Various factors, including fines content and grain characteristics influence SPT results, as noted in Table 3.1. The equation used for these corrections is:

$$(N_1)_{60} = N_m \times C_N \times C_E \times C_B \times C_R \times C_S$$

$$C_N = \left(\frac{P_a}{\sigma'_{vo}}\right)^{0.5}$$

where CN normalizes Nm to an effective overburden pressure σ_{vo}' of nearly 100 kPa (1 atm) Pa.

For magnitude scaling factor:

$$\mathrm{MSF} = \frac{10^{2.24}}{\mathrm{M_w^{2.56}}}$$

To conclude, the safety factor is determined by calculating it using the following formula.

$$\mathrm{FS} = \left(\frac{\mathrm{CRR_{7.5}}}{\mathrm{CSR}}\right) \times \mathrm{MSF}$$

where CSR, calculated cyclic stress ratio formed by the earthquake and $\mathrm{CRR_{7.5}}$, cyclic resistance ratio for magnitude 7.5 earthquakes.

3.2.4 MSF-Corrected CSR Evaluation (CSR× iMSF)

Following the liquefaction analyses based on Youd et al. (2001), an evaluation was performed by normalizing the CSR values with MSF to explicitly count on magnitude impacts. The uncertainties of the input parameters used in the CSR calculation were converted to standard deviations as suggested by Juang et al. (2008b) in Table 3.2. The uncertainty associated with PGA was obtained from the ground motion prediction model of Akkar et al. (2014) shown in Table 3.2 and combined with the uncertainties of the remaining CSR input parameters. The resulting CSR uncertainty was included in the probabilistic liquefaction hazard analysis. Then, a magnitude scaling factor was derived from the ratio of the CSR values in two liquefaction hazard curves corresponding to the same overshoot probability and finally, the moment magnitude was determined using the inverse solution of the MSF-M_w relationship. The CSR/MSF used in this study is a corrected cyclic stress ratio that includes the effect of moment magnitude and provides a better representation of the liquefaction demand because it also includes the magnitude (duration) effect. The basic relationships used in determining moment magnitude values are given in Figure 3.10.

Table 3.2. Uncertainty coefficients from Juang et al. (2008) and Akkar et.al. (2014).

Parameters	**σ**
PGA (from Akkar et al.2014)	0.6201
σ_v (from Juang et.al.2008)	0.1245
MSF (from Juang et.al.2008)	0.0749
σ_v' (from Juang et.al.2008)	0.1245

$$\ln \ln (Y) = \ln[Y_{REF}(M_W, R, SoF)] + \ln \ln [S(V_{S30}, PGA_{REF})] + \varepsilon\sigma$$

Figure 3.9. Akkar et al. (2014) ground motion prediction equation

$$CSR = \left(0.65 \times \frac{PGA}{g} \times \left(\frac{\sigma_v}{\sigma_v'}\right) \times r_d\right) \qquad MSF_{target} = \frac{CSR}{CSR \times iMSF}$$

$$CSR \times iMSF = CSR/MSF \qquad Mw_{target} = \exp\left[\frac{\ln\left(\frac{10^{2.24}}{MSF_{target}}\right)}{2.56}\right]$$

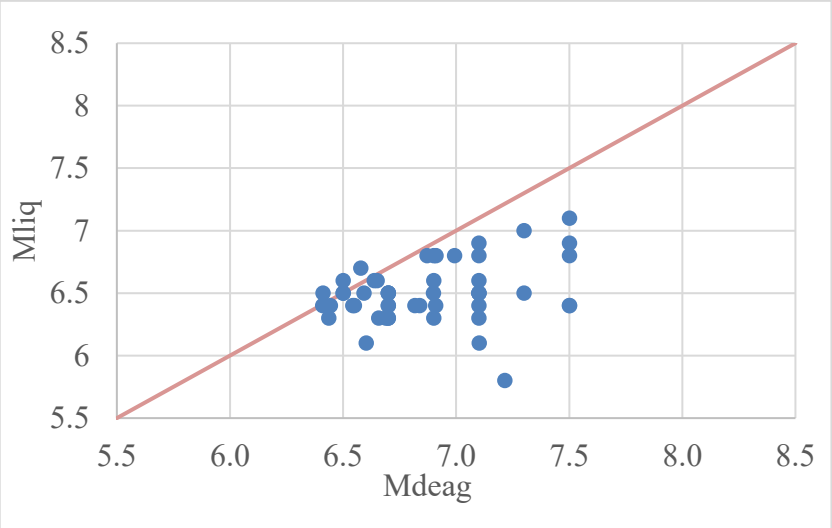
Figure 3.10. Basic relationships used in determining M_{liq} values.

4. RESULTS

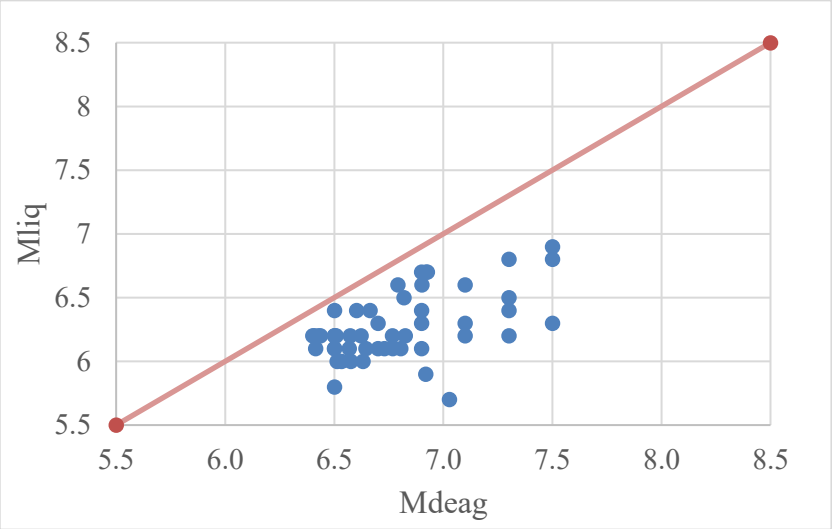
The results of the analyses are presented in this section to compare the effects of different magnitude selection methods on seismic demand and liquefaction potential. A comparative analysis of M_w values for DD-1 and DD-2 levels was performed using four different methods. The results show that M_{char} consistently produces the highest magnitude values, followed by M_{fault} while M_{deag} and M_{liq} yield lower values. In particular, the M_{liq} values are significantly lower than those obtained from the other methods. Although the values differ between the DD-1 and DD-2 risk levels, the relative ranking between the methods remains consistent. When all these comparisons are considered together, it becomes clear that moment magnitude varies depending on the purpose of the analysis and cannot be represented by a single magnitude value.

$$M_{char} > M_{fault} > M_{deag} > M_{liq}$$

Figure 4.1. compares deaggregation-based magnitudes with liquefaction hazard-based magnitudes. The results shows that, for both hazard levels, liquefaction hazard-based magnitudes are generally lower than deaggregation-based magnitudes. This indicates that the liquefaction hazard-based approach tends to yield systematically lower magnitude estimates, particularly for the DD-2 hazard level.



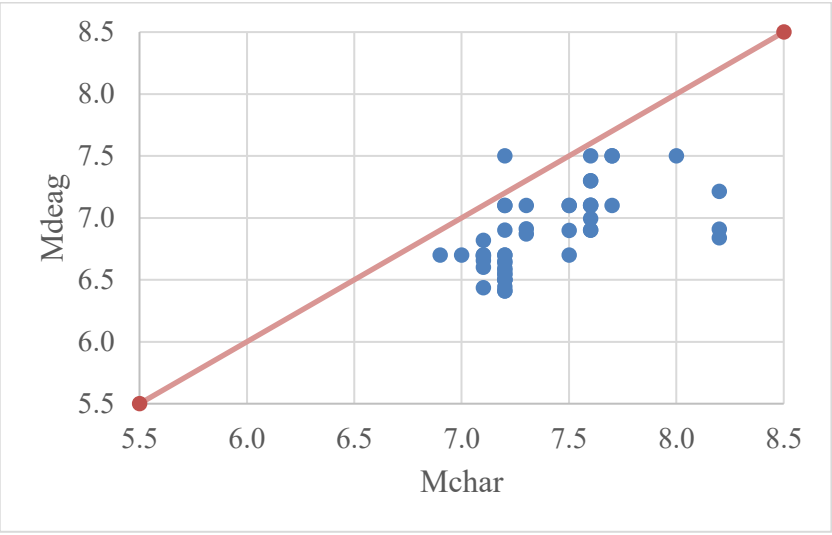
(a)



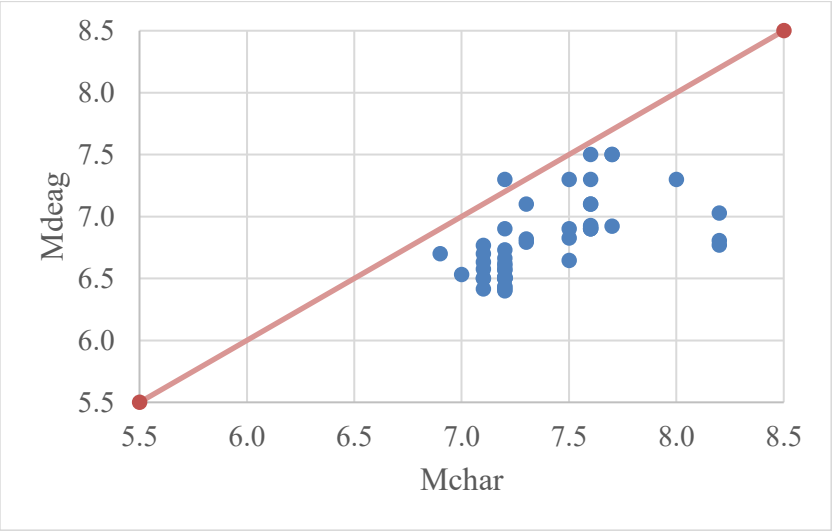
(b)

Figure 4.1. Comparison of Deaggregation-Based and Liquefaction Hazard-Based Magnitudes for (a) DD-1 and (b) DD-2 hazard levels.

Figure 4.2. compares characteristic magnitudes with deaggregation-based magnitudes. The results show that deaggregation magnitudes are mostly lower than characteristic magnitudes. This indicates that seismic hazard is controlled not only by maximum fault potential but also by earthquake scenarios with lower magnitudes but higher contributions.



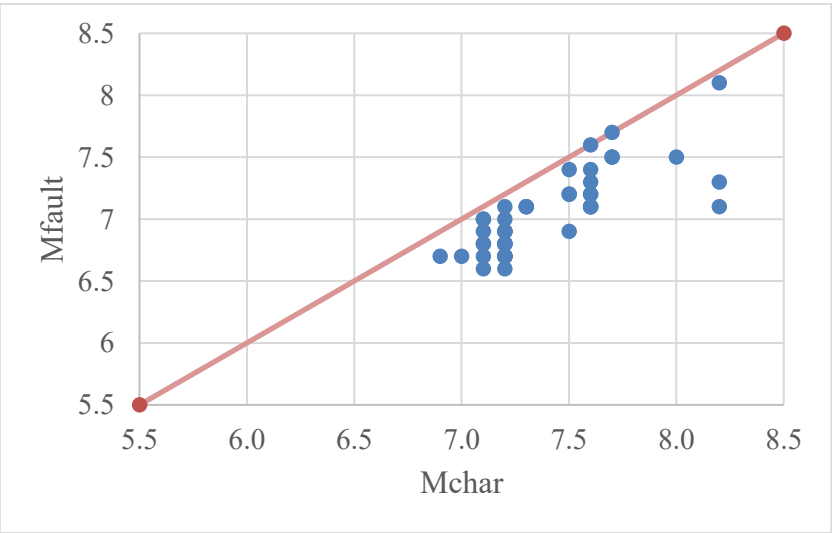
(a)



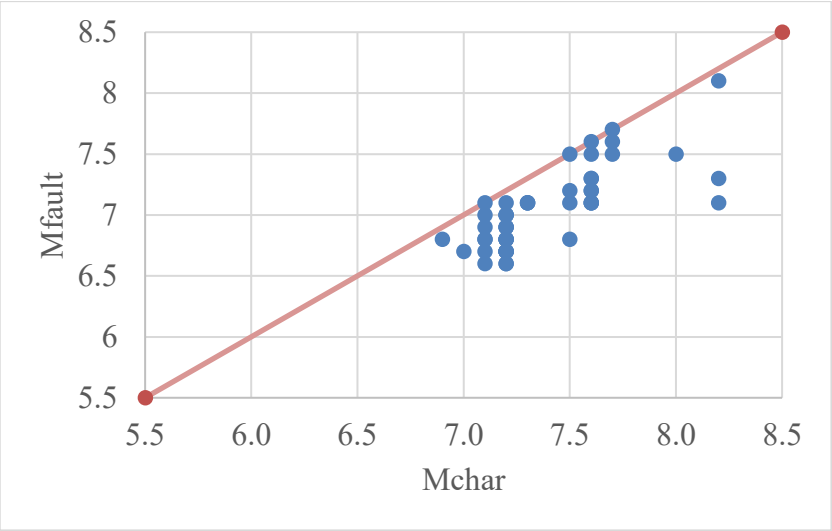
(b)

Figure 4.2. Comparison of Deaggregation-Based and Characteristic Magnitudes for (a) DD-1 and (b) DD-2 hazard levels.

Figure 4.3. compares characteristic magnitudes with magnitudes based on fault contribution. The results show that magnitudes based on fault contribution are lower than characteristic magnitudes. This indicates that faults contribute to seismic hazard through lower magnitude earthquakes rather than their maximum potential.



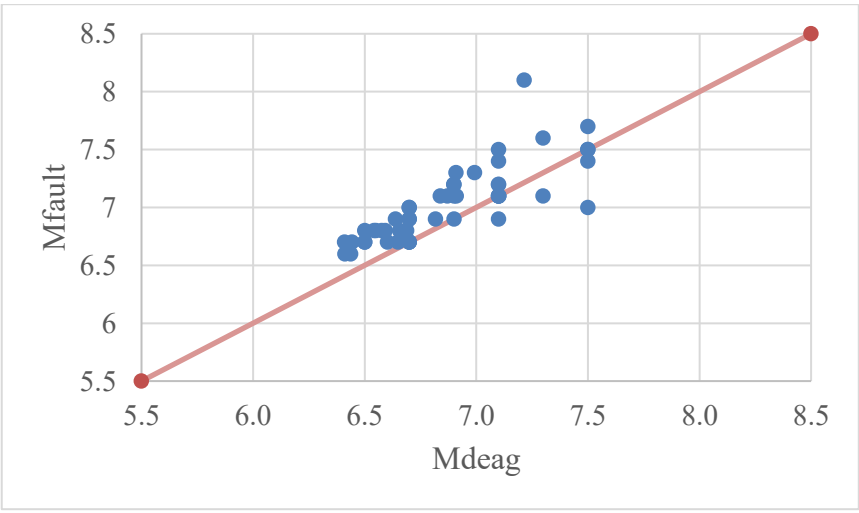
(a)



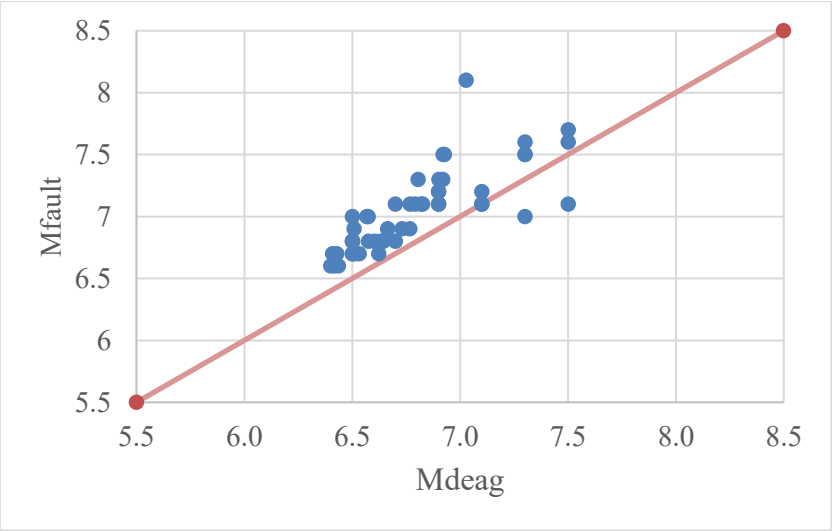
(b)

Figure 4.3. Comparison of Fault Contribution-Based and Characteristic Magnitudes for (a) DD-1 and (b) DD-2 hazard levels.

Figure 4.4. compares magnitudes based on fault contribution with magnitudes based on deaggregation. The results show a generally consistent relationship between the two types of magnitudes but magnitudes based on fault contribution generally yield higher values. This suggests that the contribution of specific faults to seismic hazard can be expressed with higher magnitudes compared to the average hazard representation.



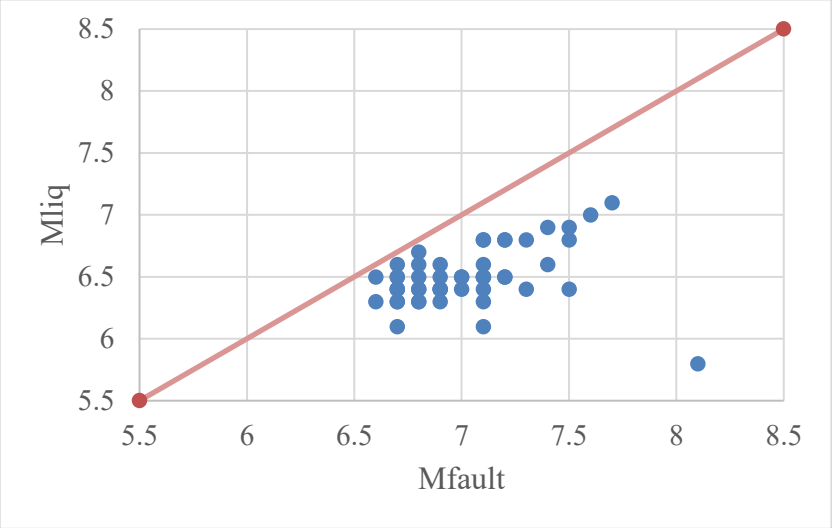
(a)



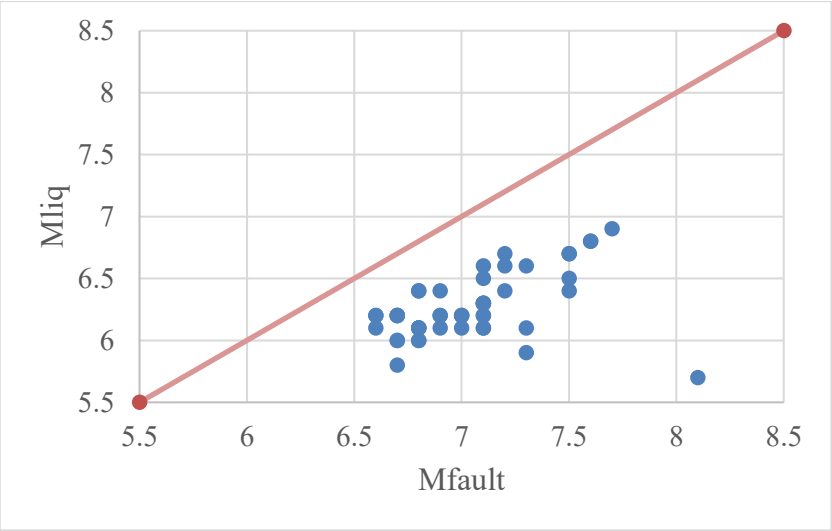
(b)

Figure 4.4. Comparison of Fault Contribution-Based and Deaggregation-Based Magnitudes for (a) DD-1 and (b) DD-2 hazard levels.

Figure 4.5. compares magnitudes based on fault contribution with magnitudes based on liquefaction analysis. The results show that liquefaction hazard-based magnitudes are systematically lower than fault contribution-based magnitudes.



(a)



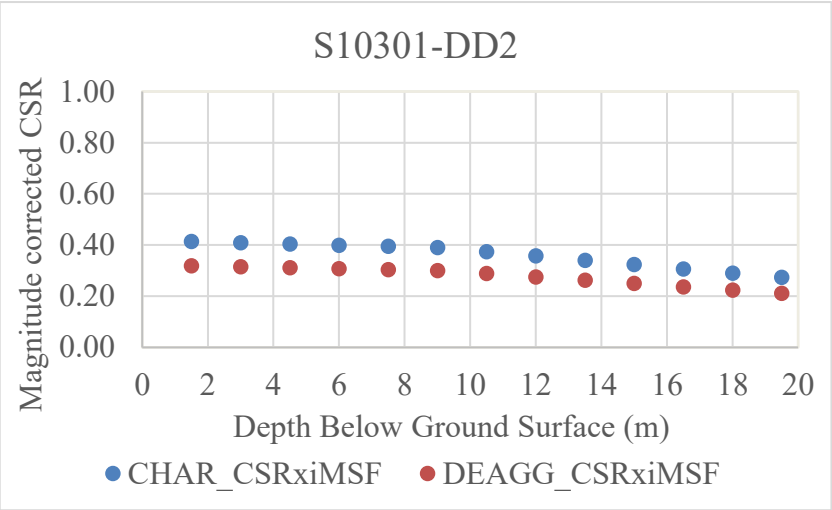
(b)

Figure 4.5. Comparison of Fault Contribution-Based and Liquefaction Hazard-Based Magnitudes for (a) DD-1 and (b) DD-2 hazard levels.

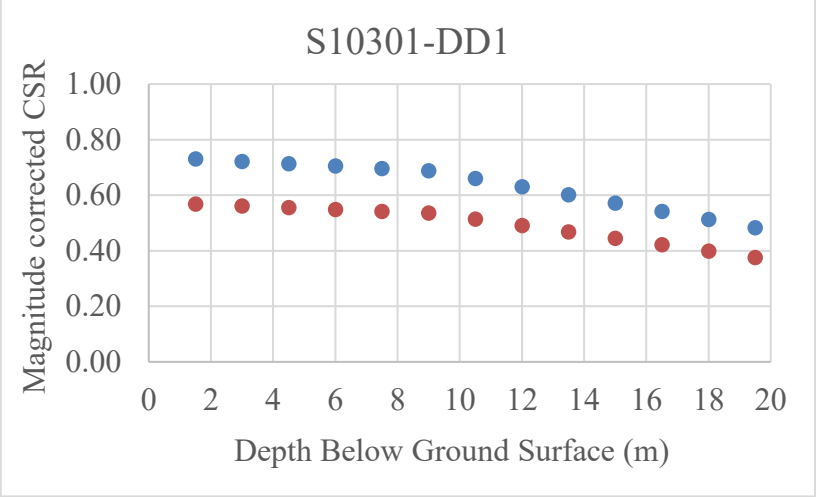
4.1 The Effect of Magnitude Selection Methods on CSR×iMSF Values

To investigate the effect of different moment magnitude selection methods on liquefaction analysis, comparative analyses were performed using characteristic magnitude, deaggregation-based magnitude, fault contribution-based magnitude and liquefaction hazard-based magnitude. The results show that there are significant differences in magnitude-corrected CSR values representing seismic demand depending on the selected magnitude method. In particular, it was observed that the M_{char} and M_{fault} methods produced higher magnitudes and therefore higher CSR values, while the M_{deag} and especially the M_{liq} methods resulted in lower seismic demand. This situation reveals that the selection of moment magnitude to be utilized in liquefaction analyses directly affects the analysis results.

Figure 4.6. compares the magnitude-corrected CSR values as a function of depth. The results show that CSR values decrease as depth increases for both hazard levels. Furthermore, it is observed that CSR values calculated based on characteristic magnitude are systematically higher than those calculated based on deaggregation. This indicates that the use of characteristic magnitude increases the liquefaction demand in a conservative direction.



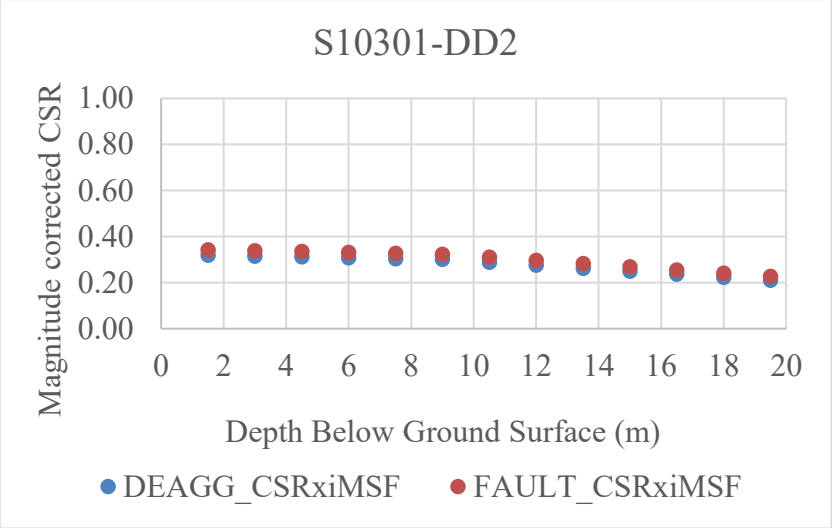
(a)



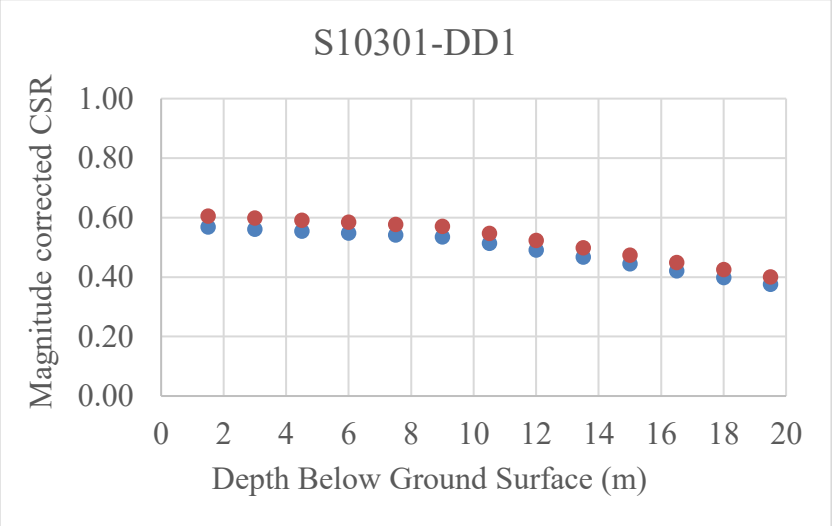
(b)

Figure 4.6. Variation of CSR×iMSF values with depth for M_{char} and M_{deag} methods at (a) DD-2 and (b) DD-1 hazard levels.

Figure 4.7 compares CSR×iMSF values calculated using deaggregation-based magnitudes and fault-contribution-based magnitudes. The results indicate that both approaches yield distributions that almost overlap along the depth profile. This suggests that both magnitude definitions produce similar results regarding liquefaction demand.



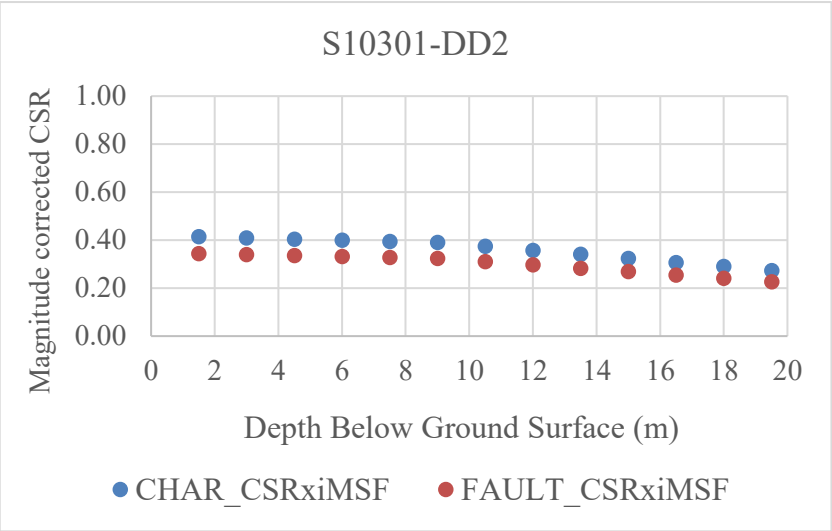
(a)



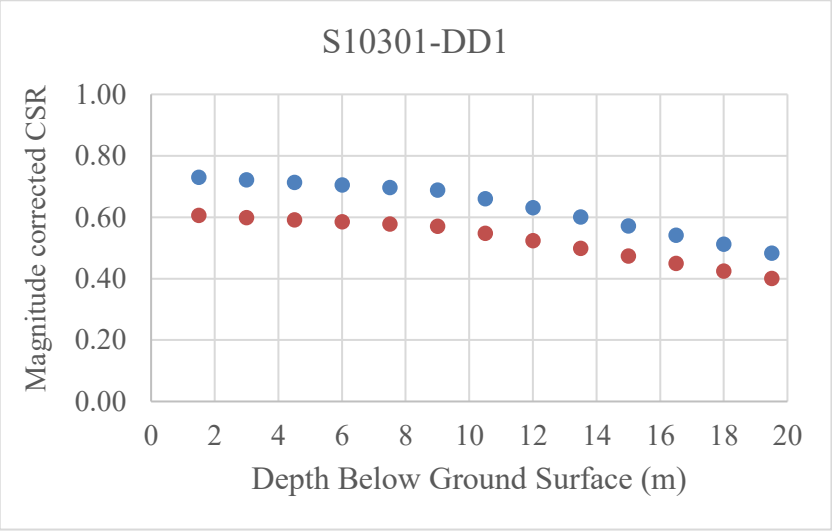
(b)

Figure 4.7. Variation of CSR×iMSF values with depth for M_{fault} and M_{deag} methods at (a) DD-2 and (b) DD-1 hazard levels.

Figure 4.8. compares the CSR×iMSF values calculated using characteristic magnitude and fault contribution-based magnitudes. The results show that the CSR values calculated based on characteristic magnitude are systematically higher than those calculated based on fault contribution. This indicates that the characteristic magnitude approach increases the liquefaction demand in a conservative direction.



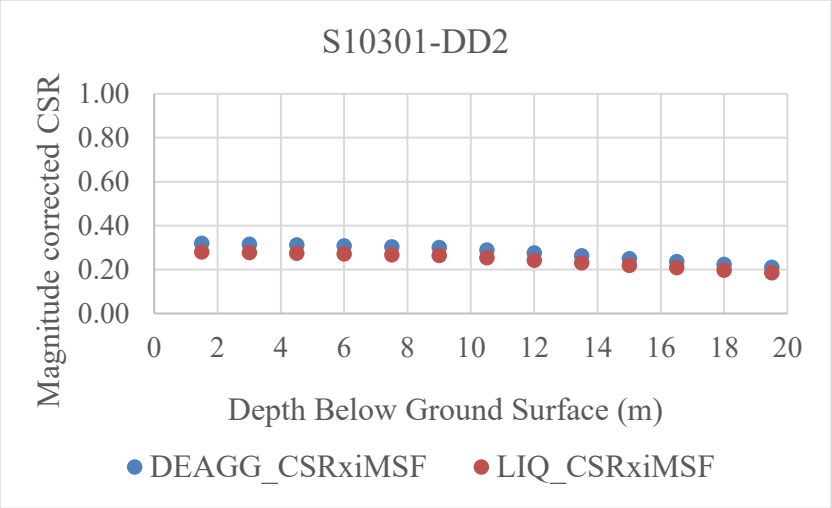
(a)



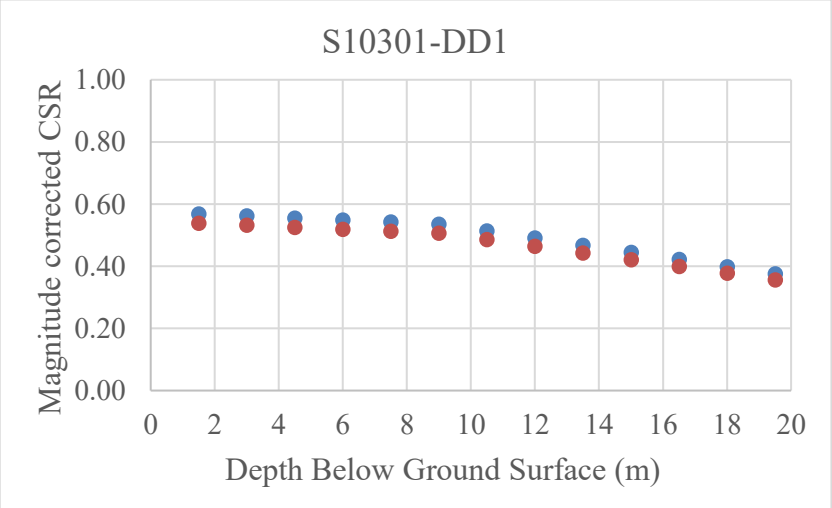
(b)

Figure 4.8. Variation of CSR×iMSF values with depth for M_{char} and M_{fault} methods at (a) DD-2 and (b) DD-1 hazard levels.

Figure 4.9. compares magnitude-corrected CSR values obtained using deaggregation-based and liquefaction hazard-based magnitudes. CSR values calculated using the liquefaction hazard-based magnitude are slightly lower than those obtained using the deaggregation-based magnitude. Although the difference between M_{liq} and M_{deag} may be significant, the resulting differences in magnitude-corrected CSR values are relatively small. This indicates that the differences between the two magnitude estimates have a limited effect on the final CSR via the MSF correction.



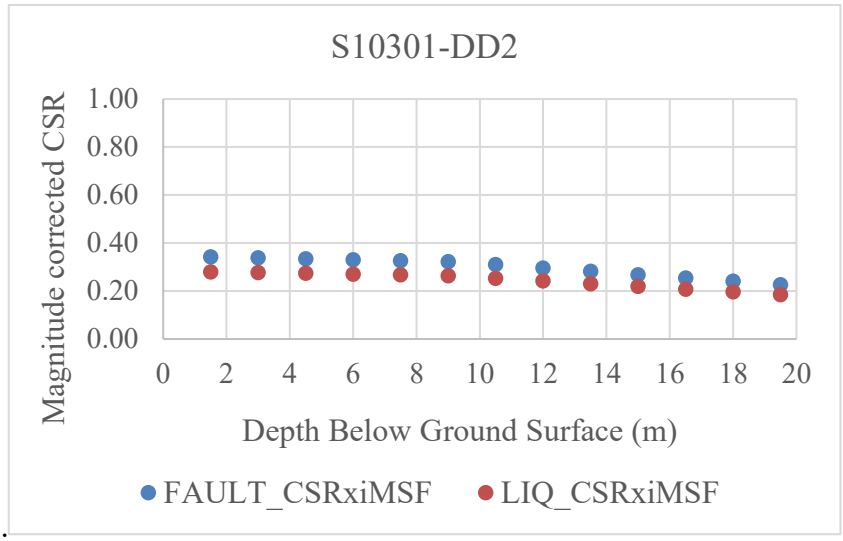
(a)



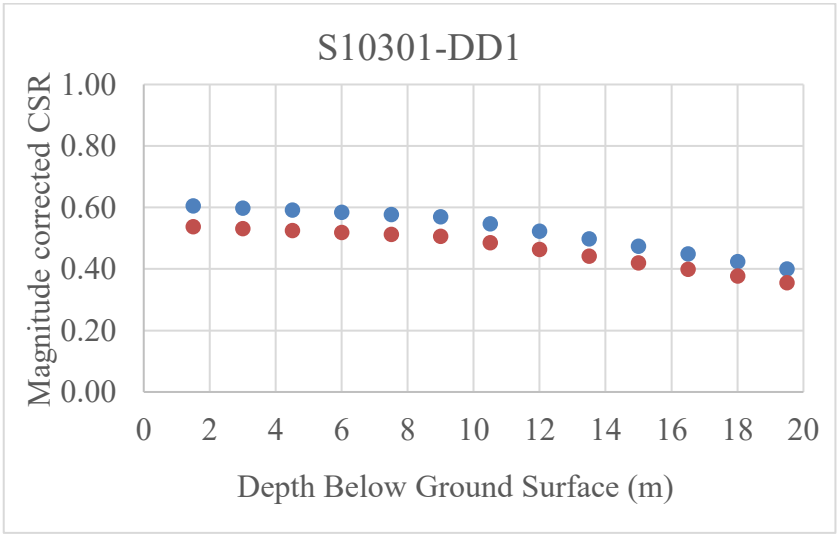
(b)

Figure 4.9. Variation of CSR×iMSF values with depth for M_{liq} and M_{deag} methods at (a) DD-2 and (b) DD-1 hazard levels.

Figure 4.10 compares magnitude-corrected CSR values obtained using fault-based and liquefaction hazard-based magnitudes. In the soil profile, M_{fault} values are consistently higher than those obtained using M_{liq}. Although both approaches exhibit a similar trend of decrease with depth, a systematic difference is observed between the methods.



(a)



(b)

Figure 4.10. Variation of CSR×iMSF values with depth for M_{fault} and M_{liq} methods at (a) DD-2 and (b) DD-1 hazard levels.

5. CONCLUSION

In this study, different approaches for selecting moment magnitude in liquefaction potential assessment were examined. The effect of moment magnitude selection on seismic demand was assessed by comparing magnitude-corrected cyclic stress ratio values obtained using four different methods: characteristic magnitude, deaggregation-based magnitude, fault contribution-based magnitude and liquefaction hazard-based magnitude.

The results show that there are significant numerical differences between the obtained M_w values depending on the magnitude selection method and these values have a direct and critical effect on the calculated seismic demand and therefore on the estimated liquefaction potential.

When all comparisons are evaluated M_{char} and M_{fault} generally yield the highest magnitude values, while M_{liq} despite being theoretically correct yields the lowest values due to its PGA-based structure. In contrast, M_{deag} yields provides average magnitude estimates among these approaches. Consequently, based on the findings of this study, the deaggregation-based moment magnitude approach is recommended for liquefaction assessment.

The main conclusions of this study are listed below:

- The M_{char} method produced the highest magnitude and consequently the highest CSR values in all analyses, representing the most conservative approach. In contrast, the M_{liq} method yielded the lowest magnitude and CSR values.

- The M_{fault} and M_{deag} methods are located between M_{char} and M_{liq}, offering more average results representing fault contributions and dominant earthquake scenarios, respectively.
- Based on the findings of the study, the deaggregation-based moment magnitude approach is recommended as the most suitable approach for liquefaction assessments.
- It has been observed that the differences between the different magnitude selection methods continue systematically throughout the depth.

- Analyses performed for DD-1 and DD-2 hazard levels showed that the absolute seismic demand values changed but the relative ranking between the methods did not change. This reveals that the effect of magnitude selection is generally systematic, regardless of the hazard level.
- The results obtained show that moment magnitude selection is not only an input parameter but also a fundamental factor directly affecting the outcome of the liquefaction analysis.

5.1 Discussions and Recommendations for Future Work

Based on the study's findings, while the deaggregation-based moment magnitude approach is suggested as the most suitable method for liquefaction assessments, its implementation requires not only the capability to perform probabilistic seismic hazard and deaggregation analyses but also a certain level of technical knowledge and expertise. Consequently, it may not always be feasible to apply this approach directly in every engineering project. In summary, although this method is considered a valid option for determining earthquake magnitude, its practical application in engineering is subject to certain limitations due to the data and analytical processes it entails. Several aspects can be further improved in future studies. Further improvements may focus on methodology efficiency and uncertainty in magnitude selection.

Firstly, it can be applied on a broader regional scale to represent regional variability and the proposed comparison can be expanded by adding more study points.

Secondly, the impact of different soil classes and site-specific parameters on magnitude selection can be investigated in more detail within the scope of these methods.

Overall, these improvements can contribute to a better and more comprehensive assessment of liquefaction hazards in future studies.

REFERENCES

Akkar, S., Sandıkkaya, M. A., & Bommer, J. J., "Empirical Ground-Motion Models for Point- and Extended-Source Crustal Earthquake Scenarios in Europe and the Middle East", Bulletin of Earthquake Engineering, Vol. 12, No. 1, pp. 359–387, **2014.**

Ambraseys, N. N., "Engineering Seismology", Earthquake Engineering and Structural Dynamics, 17, 1–105, **1988.**

Andrus, R. D., Stokoe II, K. H., "Liquefaction Resistance Based on Shear Wave Velocity", Proceedings of the NCEER Workshop on Evaluation of Liquefaction Resistance of Soils, State University of New York, Buffalo, 89–128, **1997.**

Andrus, R.D., Stokoe II, K.H., "Liquefaction Resistance of Soils from Shear-Wave Velocity", Journal of Geotechnical and Geoenvironmental Engineering, 126(11): 1015–1025, **2000.**

Andrus, R. D., Stokoe II, K. H., Juang, C. H., "Guide for Shear-Wave-Based Liquefaction Potential Evaluation", Earthquake Spectra, 20(2), 285–308, **2004.**

Arango, I., "Magnitude scaling factors for soil liquefaction evaluations", Journal of Geotechnical Engineering, ASCE, 122(11): 929–936, **1996.**

Aydoğan, B., A Method for Probabilistic Seismic Hazard Analysis of Moment Magnitude to be Used in a Liquefaction Potential Assessment, M.Sc. Thesis, Middle East Technical University, Ankara, Türkiye, **2025.**

Boulanger, R. W., Idriss, I. M., "CPT and SPT Based Liquefaction Triggering Procedures", Center for Geotechnical Modeling, University of California, Davis, Report No. UCD/CGM-14/01, 12-15, **2014.**

Bozkurt, E., "Neotectonics of Türkiye – A Synthesis", Geodinamica Acta, 14(1–3), 3–30, **2001.**

Cetin, K. O., Seed, R. B., Der Kiureghian, A., Tokimatsu, K., Harder, L. F. Jr., Kayen, R. E., Moss, R. E. S., "SPT-Based Probabilistic and Deterministic Assessment of Seismic Soil Liquefaction Potential", Journal of Geotechnical and Geoenvironmental Engineering, 130(12), 1314–1340, **2004.**

Cetin, K. O., Bilge, H. T., "Performance-Based Assessment of Magnitude (Duration) Scaling Factors", Journal of Geotechnical and Geoenvironmental Engineering, 138(3), 324–334, **2012.**

Cornell, C. A., "Engineering Seismic Risk Analysis", Bulletin of the Seismological Society of America, 58(5), 1583–1606, **1968.**

Emre, Ö., et al., "Active Fault Map of Türkiye", Maden Tetkik ve Arama Genel Müdürlüğü (MTA), Ankara**, 2013.**

Idriss, I. M., Boulanger, R. W., "Soil Liquefaction During Earthquakes", Earthquake Engineering Research Institute, MNO-12, **2008.**

Idriss, I. M., "H. B. Seed Memorial Lecture", University of California, Berkeley, **1995.**

Idriss, I. M., "An Update to the Seed-Idriss Simplified Procedure for Evaluating Liquefaction Potential", Proceedings of the TRB Workshop on New Approaches to Liquefaction, Publication No. FHWA-RD-99-165, Federal Highway Administration, Washington, DC, **1999.**

İnce, G. Ç., Yılmazoğlu, M. U., "Probabilistic Seismic Hazard Assessment of Muğla, Türkiye", Natural Hazards, **2021.**

Kayen, R., et al., "Shear-Wave Velocity–Based Probabilistic and Deterministic Assessment of Seismic Soil Liquefaction Potential", Journal of Geotechnical and Geoenvironmental Engineering, **2013.**

Kramer, S. L., "Geotechnical Earthquake Engineering", Prentice Hall, Englewood Cliffs, NJ, pp. 117–118, **1996.**

Liao, S. S. C., Whitman, R. V., "Catalogue of Liquefaction and Non-Liquefaction Occurrences during Earthquakes", Department of Civil Engineering, Massachusetts Institute of Technology (MIT), Cambridge, **1986.**

Liu, A. H., Stewart, J. P., Abrahamson, N. A., Moriwaki, Y., "Equivalent Number of Uniform Stress Cycles for Soil Liquefaction Analysis", Journal of Geotechnical and Geoenvironmental Engineering, 127(12), 1017–1026, **2001.**

McGuire, R.K., Seismic Hazard and Risk Analysis, Oakland, CA: Earthquake Engineering Research Institute, 105-142, **2004.**

Reiter, L., “Earthquake Hazard Analysis: Issues and Insights”, Columbia University Press, New York, 254 pp., **1990.**

Rockwell, T. K., Barka, A., Dawson, T., et al., “Paleoseismology of the Gazikoy-Saros Segment of the North Anatolian Fault, Northwestern Türkiye: Comparison of the Historical and Paleoseismic Records, Implications for Regional Seismic Hazard and Models of Earthquake Recurrence”, Journal of Seismology, 5(3), 433–448, **2001.**

Seed, H. B., Idriss, I. M., “Simplified Procedure for Evaluating Soil Liquefaction Potential”, Journal of the Soil Mechanics and Foundations Division, 97(9), 1249–1273, **1971.**

Seed, H. B., Idriss, I. M., “Ground Motion and Soil Liquefaction During Earthquakes”, Earthquake Engineering Research Institute Monograph, Oakland, CA, **1982.**

Sözbilir, H., Akyüz, S., Altunel, E., Gürsoy, H., “Thematic Set: Active Tectonics and Earthquake Hazard of Western Anatolia – Preface”, Turkish Journal of Earth Sciences, 17(3), 543–544, **2008.**

Youd, T. L., Idriss, I. M. andrus, R. D., et al., “Liquefaction Resistance of Soils: Summary Report from the 1996 NCEER and 1998 NCEER/NSF Workshops on Evaluation of Liquefaction Resistance of Soils”, Journal of Geotechnical and Geoenvironmental Engineering, **2001.**

Youd, T.L., Noble, S.K., “Magnitude Scaling Factors”, NCEER Workshop on Evaluation of Liquefaction Resistance of Soils, National Center for Earthquake Engineering Research, State University of New York at Buffalo, 149–165, **1997.**

APPENDIX

APPENDIX A – Seismic Hazard Analysis Outputs

siteID	lon	lat	PGA (PoE=0.1)	PGA (PoE=0.02)	SA(0.2)-0.1	SA(0.2)-0.02	SA(1.0)-0.1	SA(1.0)-0.02
10301	30.62	38.56	3.37E-01	5.95E-01	8.83E-01	1.56E+00	4.50E-01	7.82E-01
10601	31.34	40.18	2.34E-01	3.92E-01	5.96E-01	9.92E-01	5.59E-01	9.34E-01
10701	30.16	37.11	3.90E-01	6.65E-01	8.71E-01	1.46E+00	4.59E-01	8.15E-01
10702	30.74	36.89	4.02E-01	6.75E-01	8.56E-01	1.40E+00	4.18E-01	7.36E-01
10901	27.88	37.81	6.16E-01	1.07E+00	1.55E+00	2.71E+00	7.27E-01	1.27E+00
10902	27.32	37.58	5.36E-01	9.25E-01	1.34E+00	2.33E+00	6.37E-01	1.11E+00
11001	27.90	39.66	4.03E-01	7.07E-01	9.99E-01	1.73E+00	5.78E-01	9.65E-01
11002	26.99	39.53	4.96E-01	8.57E-01	1.23E+00	2.14E+00	6.89E-01	1.17E+00
11003	27.88	40.26	4.33E-01	7.35E-01	1.05E+00	1.78E+00	6.37E-01	1.04E+00
11401	31.55	40.68	8.53E-01	1.48E+00	1.87E+00	3.31E+00	1.01E+00	1.79E+00
11501	29.82	37.61	4.72E-01	7.94E-01	1.15E+00	1.94E+00	5.49E-01	9.80E-01
11601	28.40	40.08	5.11E-01	9.35E-01	1.19E+00	2.15E+00	6.57E-01	1.12E+00
11602	28.86	40.35	4.33E-01	7.37E-01	1.06E+00	1.78E+00	6.52E-01	1.06E+00
11603	28.92	39.70	3.52E-01	6.12E-01	8.93E-01	1.54E+00	5.48E-01	9.09E-01
11604	28.99	40.20	4.32E-01	7.55E-01	1.05E+00	1.82E+00	6.40E-01	1.06E+00
11605	29.51	40.09	3.62E-01	6.41E-01	9.14E-01	1.63E+00	5.95E-01	9.76E-01
11701	26.46	40.12	3.66E-01	6.21E-01	9.27E-01	1.56E+00	6.56E-01	1.07E+00
11702	26.41	39.74	4.09E-01	7.01E-01	1.02E+00	1.72E+00	6.38E-01	1.05E+00
11703	27.17	40.22	3.95E-01	6.73E-01	9.77E-01	1.66E+00	6.42E-01	1.05E+00
12001	29.06	37.57	4.39E-01	7.49E-01	1.12E+00	1.91E+00	5.48E-01	9.56E-01
12002	29.08	37.80	5.31E-01	9.08E-01	1.35E+00	2.32E+00	6.25E-01	1.09E+00
12003	29.76	38.28	4.27E-01	7.78E-01	1.08E+00	1.99E+00	5.27E-01	9.24E-01
12201	26.63	40.84	3.93E-01	6.74E-01	9.78E-01	1.67E+00	6.74E-01	1.13E+00
12601	30.52	39.76	3.43E-01	7.01E-01	8.36E-01	1.64E+00	5.29E-01	9.08E-01
13201	30.58	37.82	3.84E-01	6.65E-01	9.46E-01	1.64E+00	4.64E-01	8.28E-01
13401	28.72	40.99	5.65E-01	9.16E-01	1.34E+00	2.20E+00	7.96E-01	1.33E+00
13501	27.24	38.46	5.00E-01	8.42E-01	1.29E+00	2.19E+00	6.49E-01	1.10E+00
13502	27.33	39.17	4.96E-01	8.66E-01	1.22E+00	2.10E+00	6.34E-01	1.11E+00
13503	27.40	38.14	4.21E-01	7.14E-01	1.11E+00	1.86E+00	6.01E-01	1.03E+00
13504	27.99	38.21	3.73E-01	6.41E-01	9.82E-01	1.67E+00	5.80E-01	9.82E-01
14101	29.42	40.82	5.92E-01	9.64E-01	1.39E+00	2.29E+00	8.33E-01	1.41E+00
14102	29.82	40.62	6.17E-01	1.00E+00	1.44E+00	2.39E+00	8.64E-01	1.47E+00
14201	31.46	38.38	4.20E-01	8.19E-01	1.05E+00	2.05E+00	4.67E-01	9.12E-01
14301	29.99	39.43	4.14E-01	8.38E-01	1.03E+00	2.08E+00	5.65E-01	1.01E+00
14302	30.14	39.02	3.95E-01	7.18E-01	1.01E+00	1.82E+00	5.01E-01	8.83E-01
14501	27.39	38.73	4.93E-01	8.28E-01	1.27E+00	2.14E+00	6.38E-01	1.09E+00
14502	27.73	38.92	4.65E-01	7.82E-01	1.21E+00	2.03E+00	6.03E-01	1.03E+00
14503	28.26	38.88	3.61E-01	6.13E-01	9.43E-01	1.60E+00	5.40E-01	9.19E-01
14801	27.63	37.08	5.12E-01	8.28E-01	1.28E+00	2.08E+00	5.88E-01	1.01E+00
14802	27.79	37.29	4.85E-01	7.86E-01	1.23E+00	1.99E+00	5.59E-01	9.48E-01
14803	28.26	36.85	5.25E-01	8.59E-01	1.27E+00	2.10E+00	6.18E-01	1.07E+00
14804	28.40	37.15	4.80E-01	8.15E-01	1.17E+00	2.02E+00	5.89E-01	1.02E+00
14805	29.21	36.63	4.96E-01	8.17E-01	1.15E+00	1.93E+00	5.87E-01	1.03E+00
15401	30.28	40.52	5.28E-01	8.81E-01	1.26E+00	2.09E+00	8.01E-01	1.34E+00
15402	30.61	41.09	3.64E-01	6.07E-01	8.74E-01	1.44E+00	6.12E-01	1.01E+00
15901	27.50	40.99	4.73E-01	7.78E-01	1.17E+00	1.92E+00	7.22E-01	1.20E+00
15902	27.94	40.98	5.01E-01	8.08E-01	1.22E+00	1.97E+00	7.47E-01	1.24E+00
16401	29.50	38.78	4.10E-01	7.12E-01	1.03E+00	1.78E+00	5.28E-01	9.25E-01
16402	29.00	38.42	3.41E-01	5.86E-01	9.04E-01	1.54E+00	5.16E-01	8.85E-01
17701	29.30	40.64	7.14E-01	1.20E+00	1.65E+00	2.77E+00	9.06E-01	1.53E+00

APPENDIX B – Deaggregation Analysis Outputs

DD-1	siteID	Mmax	Mmean00	Mmean02	Mmean10	Mmode00	Mmode02	Mmode10
	10301	6.4	5.8	5.8	6.4	6.1	6.1	6.1
	10601	7.5	6.3	6.4	7.3	6.7	6.7	7.5
	10701	7.1	6.5	5.9	7.1	4.9	4.9	6.7
	10702	7.2	6.8	6.1	7.2	6.9	4.9	7.1
	10901	6.5	6.4	6.4	6.5	6.5	6.5	6.5
	10902	6.5	6.2	6.1	6.4	6.1	6.1	6.5
	11001	7.1	5.9	5.8	6.7	6.7	6.7	7.1
	11002	6.6	6.3	6.3	6.6	6.3	6.3	6.3
	11003	7.1	5.9	5.8	6.9	6.5	6.5	7.1
	11401	7.5	6.9	6.8	7.1	7.5	7.5	7.5
	11501	6.7	6.1	6.0	6.6	6.7	6.7	6.7
	11601	6.6	6.5	6.4	6.6	6.5	6.5	6.5
	11602	7.1	5.9	5.8	6.9	6.5	6.7	7.1
	11603	6.8	6.0	5.9	6.8	6.7	6.7	6.7
	11604	6.9	6.3	6.2	6.8	6.7	6.7	6.9
	11605	7.3	6.1	6.1	6.9	6.1	6.1	7.3
	11701	7.1	6.1	6.1	7.0	6.1	7.1	7.1
	11702	6.9	5.7	5.7	6.9	6.7	6.7	6.7
	11703	7.1	6.0	6.0	6.9	6.3	6.3	7.1
	12001	6.7	5.6	5.5	6.6	5.5	5.5	6.7
	12002	6.4	6.1	6.1	6.4	6.1	6.1	6.3
	12003	6.4	6.2	6.2	6.4	6.1	6.1	6.3
	12201	7.0	6.3	6.2	7.0	6.9	6.9	6.9
	12601	7.5	6.3	6.3	6.9	6.1	6.1	7.5
	13201	6.7	6.1	5.8	6.6	6.1	6.1	6.7
	13401	7.1	6.6	6.6	6.9	6.9	6.9	7.1
	13501	6.4	6.0	6.0	6.4	6.3	6.1	6.1
	13502	6.7	5.7	5.7	6.7	6.1	6.1	6.1
	13503	6.6	5.6	5.6	6.6	5.3	5.3	6.5
	13504	6.7	5.7	5.6	6.7	5.3	4.9	6.7
	14101	7.5	6.7	6.7	7.1	7.5	6.9	7.5
	14102	7.3	6.8	6.8	7.1	6.9	6.9	7.3
	14201	6.7	6.4	6.4	6.5	6.7	6.7	6.7
	14301	6.7	6.4	6.4	6.6	6.1	6.1	6.7
	14302	6.7	5.7	5.7	6.7	6.1	6.1	6.5
	14501	6.5	6.0	6.0	6.5	6.1	6.3	6.5
	14502	6.5	5.9	5.8	6.5	6.5	6.5	6.5
	14503	6.9	5.5	5.4	6.7	5.3	4.9	6.9
	14801	6.7	6.0	5.7	6.7	5.9	6.1	6.5
	14802	6.6	5.8	5.6	6.6	5.7	5.7	6.5
	14803	6.8	6.3	5.9	6.8	6.7	6.7	6.7
	14804	6.7	6.3	6.1	6.7	6.1	6.1	6.7
	14805	6.9	6.1	5.8	6.9	5.7	5.7	6.3
	15401	7.1	6.6	6.6	7.0	6.9	6.9	7.1
	15402	7.5	5.7	5.7	7.1	5.5	5.5	7.5
	15901	6.9	6.4	6.4	6.9	6.7	6.7	6.7
	15902	6.9	6.5	6.5	6.9	6.7	6.7	6.7
	16401	6.6	6.1	6.0	6.6	6.5	6.5	6.5
	16402	7.1	5.6	5.6	6.7	5.7	4.9	7.1
	17701	6.9	6.6	6.6	6.9	6.9	6.9	6.9

APPENDIX B – Deaggregation Analysis Outputs (continued)

DD-2	siteID	Mmax	Mmean00	Mmean02	Mmean10	Mmode00	Mmode02	Mmode10
	S10301	6.4	5.8	5.8	6.4	6.1	6.1	6.1
	S10601	7.5	6.5	6.5	7.1	6.9	6.9	7.5
	S10701	6.9	6.3	6.0	6.9	4.7	4.7	6.7
	S10702	7.0	6.6	6.2	7.0	6.1	4.7	6.7
	S10901	6.5	6.3	6.3	6.5	6.5	6.1	6.5
	S10902	6.4	6.0	5.9	6.4	6.3	6.3	6.1
	S11001	6.7	5.7	5.7	6.7	6.1	6.1	6.7
	S11002	6.6	6.2	6.2	6.6	6.3	6.3	6.3
	S11003	7.1	5.8	5.8	6.8	6.3	6.3	7.1
	S11401	7.5	6.8	6.8	7.0	7.5	7.5	7.5
	S11501	6.7	6.0	5.8	6.5	6.3	6.3	6.7
	S11601	6.7	6.3	6.2	6.7	6.5	6.1	6.5
	S11602	7.1	5.8	5.8	6.8	6.9	6.5	7.1
	S11603	6.8	5.8	5.8	6.8	6.3	6.3	6.7
	S11604	6.9	6.1	6.0	6.8	6.9	6.7	6.7
	S11605	7.5	6.0	6.0	6.8	6.1	6.1	7.5
	S11701	7.3	6.1	6.1	7.0	7.3	7.3	7.3
	S11702	6.8	5.7	5.7	6.8	6.7	6.7	6.7
	S11703	6.9	5.9	5.9	6.8	6.3	6.3	6.9
	S12001	6.5	5.5	5.4	6.5	5.3	4.7	6.5
	S12002	6.4	6.0	5.9	6.4	6.1	6.1	6.1
	S12003	6.4	6.1	6.1	6.4	6.1	6.1	6.1
	S12201	6.9	6.2	6.2	6.9	6.9	6.5	6.7
	S12601	7.3	6.2	6.1	6.9	6.1	6.1	7.3
	S13201	6.5	6.0	5.8	6.5	6.1	6.1	6.5
	S13401	7.1	6.5	6.5	6.8	7.1	7.1	6.9
	S13501	6.4	5.9	5.9	6.4	6.1	6.1	6.1
	S13502	6.6	5.6	5.5	6.6	6.1	6.1	6.1
	S13503	6.5	5.6	5.5	6.5	4.7	4.7	6.5
	S13504	6.6	5.7	5.7	6.6	4.7	4.7	6.5
	S14101	6.9	6.6	6.5	6.9	6.9	6.9	6.9
	S14102	7.3	6.7	6.6	6.9	7.3	6.5	7.1
	S14201	6.5	6.3	6.2	6.5	6.5	6.5	6.5
	S14301	6.7	6.3	6.3	6.6	6.1	6.1	6.7
	S14302	6.6	5.7	5.6	6.6	6.5	6.1	6.3
	S14501	6.5	5.9	5.8	6.5	6.1	6.1	6.5
	S14502	6.5	5.7	5.6	6.5	6.5	6.5	6.5
	S14503	6.6	5.4	5.4	6.6	5.1	4.7	6.3
	S14801	6.6	5.8	5.6	6.6	6.1	4.7	6.3
	S14802	6.5	5.6	5.4	6.5	4.7	4.7	6.5
	S14803	6.8	6.2	5.9	6.8	6.1	6.1	6.7
	S14804	6.6	6.2	6.0	6.6	6.1	6.1	6.5
	S14805	6.8	6.0	5.8	6.8	5.7	4.7	6.7
	S15401	6.9	6.6	6.6	6.9	6.7	6.5	6.9
	S15402	7.3	5.7	5.8	7.0	5.5	7.1	7.3
	S15901	6.8	6.3	6.2	6.8	6.7	6.5	6.7
	S15902	6.8	6.4	6.4	6.8	6.7	6.7	6.7
	S16401	6.5	6.0	5.9	6.5	6.5	6.3	6.5
	S16402	6.9	5.6	5.6	6.6	4.7	4.7	6.9
	S17701	6.9	6.6	6.5	6.8	6.9	6.9	6.9

APPENDIX C – Fault Contribution Analysis Outputs

DD-1	siteID	Mmax	Mmean00	Mmean02	Mmean10
	S10301	6.6	6.5	6.5	6.6
	S10601	7.5	7.5	7.4	7.5
	S10701	7.1	6.9	6.9	7.1
	S10702	8.1	8.1	8	7.7
	S10901	6.8	6.7	6.7	6.8
	S10902	6.7	6.6	6.6	6.7
	S11001	6.9	6.8	6.8	6.9
	S11002	6.8	6.7	6.7	6.8
	S11003	7.1	6.9	6.9	7.1
	S11401	7.7	7.7	7.7	7.6
	S11501	6.7	6.7	6.7	6.7
	S11601	6.9	6.9	6.9	6.9
	S11602	7.1	6.9	6.9	7.1
	S11603	6.9	6.8	6.8	6.9
	S11604	7.1	6.9	6.9	7.1
	S11605	7.1	6.7	6.7	7.1
	S11701	7.4	7.4	7.4	7.4
	S11702	7.2	7	7	7.2
	S11703	7.2	6.9	6.9	7.2
	S12001	6.7	6.5	6.5	6.7
	S12002	6.6	6.6	6.5	6.6
	S12003	6.7	6.7	6.7	6.7
	S12201	7.3	7.3	7.3	7.3
	S12601	7	7	7	7
	S13201	6.7	6.6	6.6	6.7
	S13401	7.2	7.2	7.2	7.2
	S13501	6.7	6.6	6.6	6.7
	S13502	6.7	6.4	6.4	6.7
	S13503	6.8	6.8	6.8	6.8
	S13504	6.9	6.9	6.9	6.9
	S14101	7.4	7.4	7.4	7.4
	S14102	7.6	7.6	7.6	7.5
	S14201	7	7	7	6.9
	S14301	7	7	7	7
	S14302	6.8	6.6	6.7	6.8
	S14501	6.7	6.6	6.6	6.7
	S14502	6.8	6.7	6.7	6.8
	S14503	6.9	6.9	6.9	6.9
	S14801	6.8	6.7	6.7	6.8
	S14802	6.7	6.6	6.6	6.7
	S14803	7.1	7	6.9	7.1
	S14804	6.9	6.7	6.7	6.9
	S14805	7.3	7.3	6.9	7.1
	S15401	7.5	7.4	7.4	7.5
	S15402	7.5	7.2	7.3	7.5
	S15901	7.1	7.1	7.1	7.1
	S15902	7.1	7	7	7.1
	S16401	6.8	6.8	6.8	6.8
	S16402	7.1	7.1	7	7
	S17701	7.2	7	7.1	7.2

APPENDIX C – Fault Contribution Analysis Outputs (continued)

DD-2	siteID	Mmax	Mmean00	Mmean02	Mmean10
	S10301	6.6	6.4	6.5	6.6
	S10601	7.6	7.5	7.5	7.6
	S10701	7.3	6.8	6.8	7.3
	S10702	8.1	8.1	8.1	7.7
	S10901	6.8	6.7	6.7	6.8
	S10902	6.6	6.6	6.6	6.6
	S11001	6.9	6.8	6.8	6.9
	S11002	6.8	6.7	6.7	6.8
	S11003	7.1	6.9	6.9	7.1
	S11401	7.7	7.7	7.7	7.7
	S11501	6.8	6.8	6.7	6.7
	S11601	6.9	6.9	6.9	6.9
	S11602	7.1	6.9	6.9	7.1
	S11603	6.9	6.8	6.8	6.9
	S11604	7.1	7	6.9	7.1
	S11605	7.1	6.6	6.6	7.1
	S11701	7.5	7.5	7.4	7.4
	S11702	7.1	7	7	7.1
	S11703	7.2	6.7	6.8	7.2
	S12001	6.7	6.3	6.4	6.7
	S12002	6.6	6.6	6.6	6.6
	S12003	6.7	6.7	6.7	6.7
	S12201	7.3	7.3	7.3	7.3
	S12601	7	7	7	7
	S13201	6.7	6.6	6.6	6.7
	S13401	7.2	7.2	7.2	7.2
	S13501	6.7	6.5	6.6	6.7
	S13502	6.7	6.4	6.4	6.7
	S13503	6.9	6.9	6.9	6.8
	S13504	7	7	6.9	6.9
	S14101	7.5	7.5	7.4	7.5
	S14102	7.6	7.5	7.6	7.6
	S14201	7	7	7	7
	S14301	7.1	7.1	7.1	7.1
	S14302	6.8	6.6	6.6	6.8
	S14501	6.7	6.6	6.6	6.7
	S14502	6.8	6.6	6.6	6.8
	S14503	7	6.8	6.8	7
	S14801	6.8	6.7	6.7	6.8
	S14802	6.7	6.6	6.6	6.7
	S14803	7.1	6.9	6.8	7.1
	S14804	6.8	6.7	6.7	6.8
	S14805	7.3	7.3	6.7	7.2
	S15401	7.5	7.3	7.3	7.5
	S15402	7.5	7	7.2	7.5
	S15901	7.1	7.1	7.1	7.1
	S15902	7.1	7	7	7.1
	S16401	6.8	6.8	6.8	6.8
	S16402	7.1	7.1	7.1	7.1
	S17701	7.2	7	7	7.2

APPENDIX D – Liquefaction Hazard- Based and Charachteristic M_w Outputs

siteID	Liq_Hzrd_DD-1	Liq_Hzrd_DD-2
S10301	6.3	6.1
S10601	6.8	6.8
S10701	6.1	5.9
S10702	5.8	5.7
S10901	6.6	6.4
S10902	6.5	6.2
S11001	6.4	6.1
S11002	6.7	6.4
S11003	6.5	6.2
S11401	7.1	6.9
S11501	6.4	6.1
S11601	6.6	6.4
S11602	6.5	6.3
S11603	6.4	6.2
S11604	6.6	6.3
S11605	6.5	6.3
S11701	6.6	6.5
S11702	6.5	6.2
S11703	6.5	6.4
S12001	6.3	6
S12002	6.5	6.2
S12003	6.4	6.2
S12201	6.8	6.6
S12601	6.4	6.2
S13201	6.3	6
S13401	6.8	6.6
S13501	6.4	6.2
S13502	6.6	6.2
S13503	6.5	6.2
S13504	6.5	6.2
S14101	6.9	6.7
S14102	7	6.8
S14201	6.5	6.2
S14301	6.5	6.3
S14302	6.3	6
S14501	6.5	6.2
S14502	6.4	6.1
S14503	6.3	6.1
S14801	6.3	6
S14802	6.1	5.8
S14803	6.4	6.1
S14804	6.4	6.1
S14805	6.4	6.1
S15401	6.9	6.7
S15402	6.4	6.4
S15901	6.8	6.5
S15902	6.8	6.6
S16401	6.4	6.1
S16402	6.3	6.1
S17701	6.8	6.7

siteID	M_{fault}
S10301	6.6
S10601	7.5
S10701	7.1
S10702	8.1
S10901	6.8
S10902	6.7
S11001	6.9
S11002	6.8
S11003	7.1
S11401	7.7
S11501	6.7
S11601	6.9
S11602	7.1
S11603	6.9
S11604	7.1
S11605	7.1
S11701	7.4
S11702	7.2
S11703	7.2
S12001	6.7
S12002	6.6
S12003	6.7
S12201	7.3
S12601	7
S13201	6.7
S13401	7.2
S13501	6.7
S13502	6.7
S13503	6.8
S13504	6.9
S14101	7.4
S14102	7.6
S14201	7
S14301	7
S14302	6.8
S14501	6.7
S14502	6.8
S14503	6.9
S14801	6.8
S14802	6.7
S14803	7.1
S14804	6.9
S14805	7.3
S15401	7.5
S15402	7.5
S15901	7.1
S15902	7.1
S16401	6.8
S16402	7.1
S17701	7.2

APPENDIX E - Comparison of M_w values

DD-1	siteID	M_{char}	M_{deag}	M_{fault}	M_{liq}
	S10301	7.1	6.4	6.6	6.3
	S10601	7.7	7.5	7.5	6.8
	S10701	7.6	7.1	7.1	6.1
	S10702	8.2	7.2	8.1	5.8
	S10901	7.2	6.5	6.8	6.6
	S10902	7.2	6.5	6.7	6.5
	S11001	7.2	7.1	6.9	6.4
	S11002	7.2	6.6	6.8	6.7
	S11003	7.3	7.1	7.1	6.5
	S11401	7.7	7.5	7.7	7.1
	S11501	6.9	6.7	6.7	6.4
	S11601	7.2	6.6	6.9	6.6
	S11602	7.6	7.1	7.1	6.5
	S11603	7.1	6.8	6.9	6.4
	S11604	7.6	6.9	7.1	6.6
	S11605	7.6	7.3	7.1	6.5
	S11701	7.5	7.1	7.4	6.6
	S11702	7.5	6.9	7.2	6.5
	S11703	7.5	7.1	7.2	6.5
	S12001	7.2	6.7	6.7	6.3
	S12002	7.2	6.4	6.6	6.5
	S12003	7.2	6.4	6.7	6.4
	S12201	7.6	7.0	7.3	6.8
	S12601	7.2	7.5	7	6.4
	S13201	7.0	6.7	6.7	6.3
	S13401	7.6	7.1	7.2	6.8
	S13501	7.2	6.4	6.7	6.4
	S13502	7.2	6.7	6.7	6.6
	S13503	7.2	6.6	6.8	6.5
	S13504	7.2	6.7	6.9	6.5
	S14101	7.6	7.5	7.4	6.9
	S14102	7.6	7.3	7.6	7
	S14201	7.1	6.7	7	6.5
	S14301	7.1	6.7	7	6.5
	S14302	7.1	6.7	6.8	6.3
	S14501	7.2	6.5	6.7	6.5
	S14502	7.2	6.5	6.8	6.4
	S14503	7.2	6.9	6.9	6.3
	S14801	7.1	6.7	6.8	6.3
	S14802	7.1	6.6	6.7	6.1
	S14803	8.2	6.8	7.1	6.4
	S14804	7.5	6.7	6.9	6.4
	S14805	8.2	6.9	7.3	6.4
	S15401	7.7	7.1	7.5	6.9
	S15402	8.0	7.5	7.5	6.4
	S15901	7.3	6.9	7.1	6.8
	S15902	7.3	6.9	7.1	6.8
	S16401	7.2	6.6	6.8	6.4
	S16402	7.2	7.1	7.1	6.3
	S17701	7.6	6.9	7.2	6.8

APPENDIX E - Comparison of M_w values (continued)

DD-2	siteID	M_{char}	M_{deag}	M_{fault}	M_{liq}
	S10301	7.1	6.4	6.6	6.1
	S10601	7.7	7.5	7.6	6.8
	S10701	7.6	6.9	7.3	5.9
	S10702	8.2	7.0	8.1	5.7
	S10901	7.2	6.5	6.8	6.4
	S10902	7.2	6.4	6.6	6.2
	S11001	7.2	6.7	6.9	6.1
	S11002	7.2	6.6	6.8	6.4
	S11003	7.3	7.1	7.1	6.2
	S11401	7.7	7.5	7.7	6.9
	S11501	6.9	6.7	6.8	6.1
	S11601	7.2	6.7	6.9	6.4
	S11602	7.6	7.1	7.1	6.3
	S11603	7.1	6.8	6.9	6.2
	S11604	7.6	6.9	7.1	6.3
	S11605	7.6	7.5	7.1	6.3
	S11701	7.5	7.3	7.5	6.5
	S11702	7.5	6.8	7.1	6.2
	S11703	7.5	6.9	7.2	6.4
	S12001	7.2	6.5	6.7	6
	S12002	7.2	6.4	6.6	6.2
	S12003	7.2	6.4	6.7	6.2
	S12201	7.6	6.9	7.3	6.6
	S12601	7.2	7.3	7	6.2
	S13201	7.0	6.5	6.7	6
	S13401	7.6	7.1	7.2	6.6
	S13501	7.2	6.4	6.7	6.2
	S13502	7.2	6.6	6.7	6.2
	S13503	7.2	6.5	6.9	6.2
	S13504	7.2	6.6	7	6.2
	S14101	7.6	6.9	7.5	6.7
	S14102	7.6	7.3	7.6	6.8
	S14201	7.1	6.5	7	6.2
	S14301	7.1	6.7	7.1	6.3
	S14302	7.1	6.6	6.8	6
	S14501	7.2	6.5	6.7	6.2
	S14502	7.2	6.5	6.8	6.1
	S14503	7.2	6.6	7	6.1
	S14801	7.1	6.6	6.8	6
	S14802	7.1	6.5	6.7	5.8
	S14803	8.2	6.8	7.1	6.1
	S14804	7.5	6.6	6.8	6.1
	S14805	8.2	6.8	7.3	6.1
	S15401	7.7	6.9	7.5	6.7
	S15402	8.0	7.3	7.5	6.4
	S15901	7.3	6.8	7.1	6.5
	S15902	7.3	6.8	7.1	6.6
	S16401	7.2	6.5	6.8	6.1
	S16402	7.2	6.9	7.1	6.1
	S17701	7.6	6.9	7.2	6.7